Active deformation near the Nicoya Peninsula, northwestern Costa Rica, between 1996 and 2010: Interseismic megathrust coupling

Lujia Feng,[1,2] Andrew V. Newman,[1] Marino Protti,[3] Víctor González,[3] Yan Jiang,[4] and Timothy H. Dixon[4,5]

Received 12 February 2012; revised 1 May 2012; accepted 14 May 2012; published 26 June 2012.

[1] We use campaign and continuous GPS measurements at 49 sites between 1996 and 2010 to describe the long-term active deformation in and near the Nicoya Peninsula, northwestern Costa Rica. The observed deformation reveals partial partitioning of the Cocos-Caribbean oblique convergence into trench-parallel forearc sliver motion and less oblique thrusting on the subduction interface. The northern Costa Rican forearc translates northwestward as a whole ridge block at 11 ± 1 mm/yr relative to the stable Caribbean. The transition from the forearc to the stable Caribbean occurs in a narrow deforming zone of ~16 km wide. Subduction thrust earthquakes take 2/3 of the trench-parallel component of the plate convergence; however, surface deformation caused by interseismic megathrust coupling is primarily trench-normal. Two fully coupled patches, one located offshore Nicoya centered at ~15 km depth and the other located inland centered at ~24 km depth, are identified in Nicoya with the potential to generate an M_w 7.8 1950-type earthquake. Another fully coupled patch SE of Nicoya coincides with the rupture region of the 1990 Nicoya Gulf earthquake. Interface microearthquakes, non-volcanic tremor, low-frequency earthquakes, and transient slow-slip events generally occur in the intermediately to weakly coupled regions.

Citation: Feng, L., A. V. Newman, M. Protti, V. González, Y. Jiang, and T. H. Dixon (2012), Active deformation near the Nicoya Peninsula, northwestern Costa Rica, between 1996 and 2010: Interseismic megathrust coupling, *J. Geophys. Res.*, *117*, B06407, doi:10.1029/2012JB009230.

1. Introduction

[2] The Nicoya Peninsula on the Pacific coast of Costa Rica in Central America is one of the closest landmasses (within 60–120 km) to the Middle America Trench (MAT). Offshore Nicoya the young oceanic Cocos plate (CO) is subducting underneath the Caribbean plate (CA) at a convergence rate of 82.3 ± 2.2 mm/yr and in a direction of N20°E ± 2° according to the GPS-based Pacific Velocity (PVEL) model by *DeMets et al.* [2010] (Figure 1).

[3] Owing to such a rapid subduction and the proximity to the trench, three devastating megathrust earthquakes (likely $M > 7.5$) have been recorded directly beneath Nicoya in 1853, 1900, and 1950, respectively, following an approximate 50-year characteristic earthquake cycle [*Protti et al.*, 2001]. However, only one large subduction thrust earthquake, the 1978 $M_w = 7.0$ Sámara earthquake, has occurred in Nicoya since 1950. The average slip of the 1978 event was estimated to be 0.7 m [*Protti et al.*, 2001] accounting for 16% of the potential accumulated slip from 1950 to 2010 assuming 100% coupling. Two recent large earthquakes bounded the peninsula. The Nicaragua subduction segment just NW of Nicoya experienced a shallow $M_w = 7.7$ tsunami earthquake in 1992 [e.g., *Kanamori and Kikuchi*, 1993; *Satake*, 1994; *Ihmlé*, 1996] and the Nicoya Gulf entrance immediately SE of Nicoya was struck by a deeper $M_w = 7.0$ event in 1990 [*Protti et al.*, 1995; *Husen et al.*, 2002; *Bilek et al.*, 2009] (Figure 1b). Neither of these two events ruptured the Nicoya segment [*Protti et al.*, 1995] indicating the Nicoya segment is a prominent seismic gap with a large 1950-type earthquake missing (Figure 1b).

[4] Warnings about the increasing risk of a large megathrust earthquake striking Nicoya have been issued for two decades [e.g., *Nishenko*, 1991; *Protti et al.*, 1995]. Until recently, the discovery of transient slow-slip events (SSE) [*Protti et al.*, 2004; *Brown et al.*, 2005; *Outerbridge et al.*, 2010; *Jiang et al.*, 2012], deep low-frequency earthquakes (LFEs) [*Brown et al.*, 2009], and non-volcanic tremor

[1]School of Earth and Atmospheric Sciences, Georgia Institute of Technology, Atlanta, Georgia, USA.
[2]Now at Earth Observatory of Singapore, Nanyang Technological University, Singapore.
[3]Observatorio Vulcanológico y Sismológico de Costa Rica, Universidad Nacional, Heredia, Costa Rica.
[4]Rosenstiel School of Marine and Atmospheric Sciences, University of Miami, Miami, Florida, USA.
[5]Now at Department of Geology, University of South Florida, Tampa, Florida, USA.

Corresponding author: L. Feng, Earth Observatory of Singapore, Nanyang Technological University, 50 Nanyang Ave., Block N2-1A-15, 639798, Singapore. (lfeng@ntu.edu.sg)

©2012. American Geophysical Union. All Rights Reserved.
0148-0227/12/2012JB009230

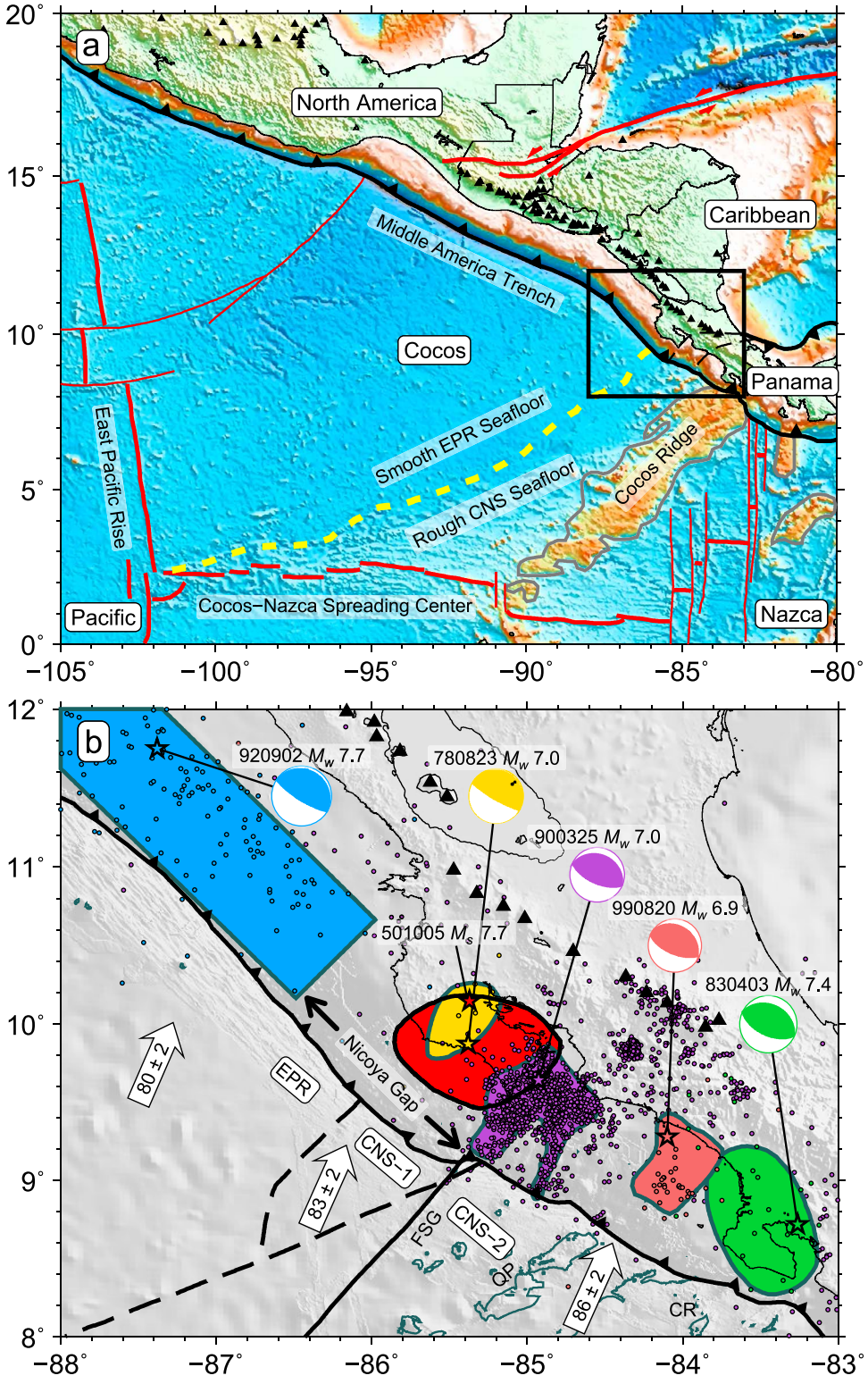
a
North America
Caribbean
Middle America Trench
Cocos
Panama
East Pacific Rise
Smooth EPR Seafloor
Rough CNS Seafloor
Cocos Ridge
Pacific
Cocos–Nazca Spreading Center
Nazca
20°
15°
10°
5°
0°
−105°
−100°
−95°
−90°
−85°
−80°
b
920902 M_w 7.7
780823 M_w 7.0
900325 M_w 7.0
990820 M_w 6.9
501005 M_s 7.7
830403 M_w 7.4
80 ± 2
EPR
Nicoya Gap
CNS-1
83 ± 2
FSG
CNS-2
QP
86 ± 2
CR
12°
11°
10°
9°
8°
−88°
−87°
−86°
−85°
−84°
−83°

Figure 1

(NVT) [*Outerbridge et al.*, 2010; *Walter et al.*, 2011] along the Nicoya segment complicated the characteristic earthquake cycle and may raise a new question; that is, whether frequent silent transient slips have secretly released the accumulated strain over the last 60 years. Nevertheless, >10 mm/yr subsidence along the coast observed by local residents [*Marshall and Anderson*, 1995] and geodetic studies [*Lundgren et al.*, 1999; *Iinuma et al.*, 2004; *Norabuena et al.*, 2004; *LaFemina et al.*, 2009] strongly suggests that the overriding plate is probably dragged down by a strong coupling with the subducting plate.

[5] To investigate if long-term strong coupling exists on the Nicoya subduction interface, we present a new interseismic megathrust coupling model based on the latest campaign and continuous GPS data between 1996 and 2010. We show that a potential $M \sim 7.8$ megathrust earthquake may occur in the fully coupled portion of the subduction interface despite that microearthquakes, NVT, LFEs, and transient slips occur in the intermediately to weakly coupled regions.

2. GPS Data and Analysis

2.1. Campaign and Continuous GPS

[6] Before 2010, previous campaigns including CASA 1994 [*Lundgren et al.*, 1999], CASA 1996 [*Lundgren et al.*, 1999], Costa Rica 2000 [*Norabuena et al.*, 2004], and Costa Rica 2003 [*LaFemina et al.*, 2009] provide a long GPS campaign history for Nicoya. Other campaigns were also carried out between 1997 and 2003 for three sites (PARK, GR38, and WARN) at Arenal Volcano, which is located east of Nicoya (Figure 2).

[7] We performed the most recent GPS campaign in early March 2010 almost doubling the observation length since the previous campaign in 2003. Twenty-four existing campaign sites in both Nicoya and Arenal were reoccupied mostly for three consecutive UTC days. Four sites (AGUS, CORO, GUAR, and LOCA) were destroyed before the 2010 campaign and CABU was missed (Figure 2). For these five stations, analyses were performed on the previous campaign data only. For the 2010 campaign, a combination of Trimble R7 and Trimble 5700 GPS receivers were used along with Trimble Zephyr Geodetic antennas. The recording interval is 15 s and the elevation mask is 5°.

[8] The Nicoya continuous GPS network was initiated in 2002 with three stations (IND1, HUA2, and PUJE) installed along a NE-SW transect in central Nicoya and completed with a total of 19 stations in late 2009 [*Outerbridge et al.*, 2010] (Figure 2). Of the continuous stations, ELVI was precluded from the following analysis because of the receiver malfunction. Likewise, PNE2 is ~50 m from previous site PNEG, but had only one fifth of PNEG's duration and thus was also excluded. Although five other sites (BIJA, CABA, EPZA, LAFE, and VERA) also had similar short duration of ~1 year (Figure A2), they were kept in the analysis on account of their unique locations. Additionally, we included two continuous GPS stations at Arenal Volcano (AROL and LOLA) from 1996 to 2003 and another continuous site (IRZU) at Irazú Volcano from late 1999 to early 2003 (Figure 2).

[9] In summary, a total of 49 GPS stations including 29 campaign sites were used in this study covering the Nicoya Peninsula and a large area NE of it (Figure 2). Time series of all the 49 stations relative to the stable Caribbean plate are provided in Appendix A (Figures A1–A3). The average time span is 7.9 years. The average station spacing is 15–20 km for Nicoya and ~30 km more inland.

2.2. GPS Data Analysis

[10] Using GIPSY 5 software from the Jet Propulsion Laboratory (JPL) along with precise satellite orbits and clocks provided by JPL [*Zumberge et al.*, 1997], all the data except the 1994 campaign that lacks JPL orbit and clock information were processed at the Geodesy Lab of the University of Miami. The resulting fiducial-free daily solutions [*Heflin et al.*, 1992] were converted to the International Terrestrial Reference Frame 2005 (ITRF2005) [*Altamimi et al.*, 2007]. To keep consistency between the campaign and continuous data, no filtering was implemented, but daily solutions with formal error larger than 3 times the average

Figure 1. (a) Regional tectonic map of Central America. Plates in this region include Cocos, Caribbean, Nazca, Panama [*Marshall et al.*, 2000], North America, and Pacific. Active spreading centers (thick red lines without arrows), fracture zones (thin red lines), the CNS-EPR boundary (yellow dashed line), and high-relief ridges (gray lines) are based on *Barckhausen et al.* [2001], *MacMillan et al.* [2004], and *Lonsdale* [2005]. Left-lateral transform faults (thick red lines with arrows) are taken from *Plafker* [1976] and *Rosencrantz and Mann* [1991]. Black triangles are volcanoes with evidence of Holocene activity [*Siebert and Simkin*, 2002]. Box outlines the area of Figure 1b. Bathymetry and topography use ETOPO2v2 Global Gridded 2-minite Database. (b) Large earthquakes in Nicoya and surrounding regions since 1950. Different color patches with stars as epicenters indicate rupture areas identified from aftershock distribution for 1950 Nicoya [*Güendel*, 1986; *Avants et al.*, 2001; *Norabuena et al.*, 2004], 1978 Nicoya [*Güendel*, 1986; *Avants et al.*, 2001; *Norabuena et al.*, 2004], 1983 Osa [*Adamek et al.*, 1987], 1990 Nicoya Gulf [*Protti et al.*, 1995], 1992 Nicaragua [*Ihmlé*, 1996], and 1999 Quepos [*DeShon et al.*, 2003] earthquakes. Circles are 3-month aftershocks from the OVSICORI seismic catalog for the 1990 event and from PDE for others. Focal mechanisms are from *Adamek et al.* [1987] for the 1983 event, from *Protti et al.* [1995] for the 1990 event, and the global centroid moment tensor (gCMT) catalog [*Ekström et al.*, 2005] for others. Historically, the Nicoya segment has the largest thrust earthquakes ($M > 7.5$) in the Pacific of Costa Rica compared to moderate-magnitude ($7 < M < 7.5$) earthquakes in southeastern Costa Rica where the Cocos Ridge subducts and smaller-magnitude ($M \sim 7$) earthquakes in central Costa Rica where abundant small isolated seamounts subduct [*Protti et al.*, 1994; *Bilek et al.*, 2003]. Cocos-Caribbean convergence vectors (mm/yr) are derived from the PVEL model by *DeMets et al.* [2010]. Dashed lines are the boundaries separating seafloor spreading magnetic anomalies into EPR, CNS-1, and CNS-2; solid line is a propagator coinciding with the Fisher Ridge [*Barckhausen et al.*, 2001]. CNS, Cocos-Nazca spreading center; EPR, East Pacific Rise spreading center; CR, Cocos Ridge; FSG, Fisher Seamount Group; QP, Quepos Plateau.

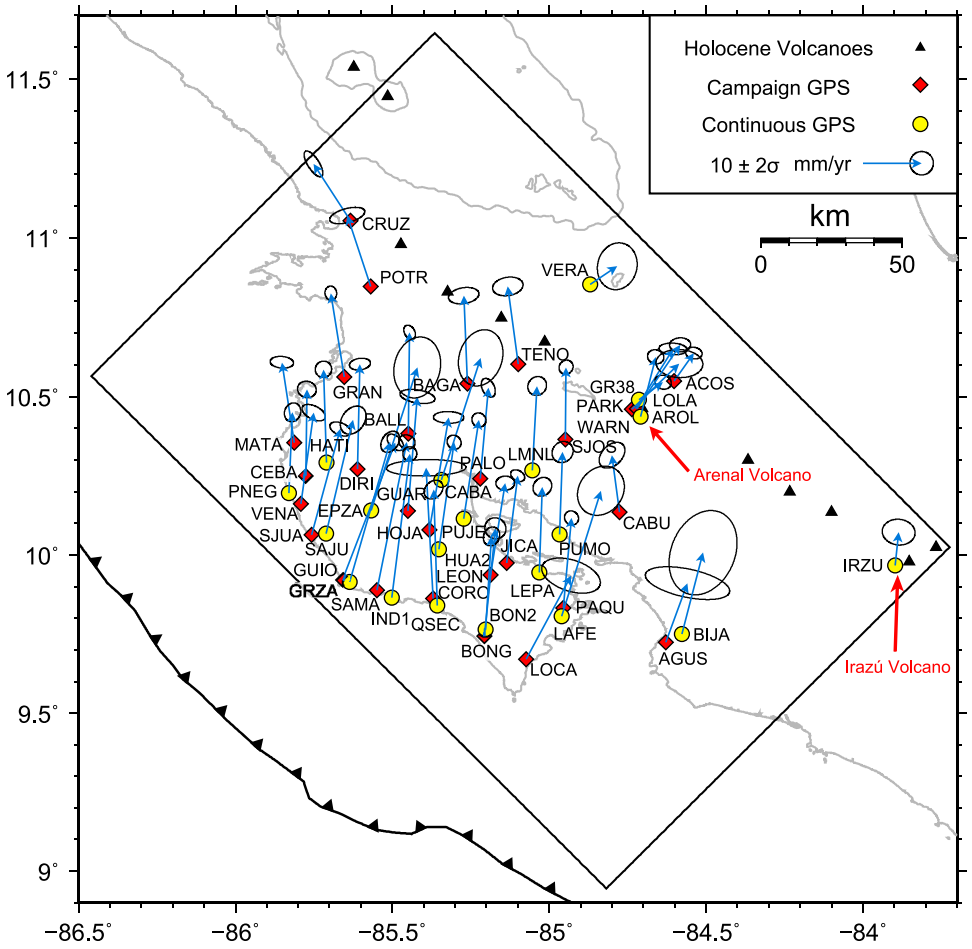

Figure 2. Map of campaign (yellow circles) and continuous (red diamonds) GPS stations. Blue vectors show horizontal velocities relative to the stable Caribbean plate [*DeMets et al.*, 2010] between 1996 and 2010. 2-D 2σ error ellipses represent 86.5% confidence. Black box outlines the bounds of Figures 3a and 4a.

error were removed as outliers. The long-term interseismic velocities were estimated by iteratively fitting straight lines through individual components of the time series using a weighted least squares method. In each iteration, outliers that have a deviation from the estimated linear trend larger than 3 times the weighted root-mean square scatter (WRMS) were flagged and removed. The best fit rates were achieved until no more outliers can be identified.

[11] The error calculation adopted an empirical noise model by *Mao et al.* [1999], which accounts for both the time-uncorrelated and time-correlated noises. Individual noise contributions for the north, east, and vertical components were separately estimated from WRMS using equations given by *Dixon et al.* [2000]. Though campaign data were clustered in a few days with very irregular spacing, the extremely long time span of the data for most sites significantly reduced uncertainties. The resulting velocities with their corresponding errors relative to ITRF2005 are listed in Table 1.

[12] Besides interseismic strain accumulation and forearc sliver motion, other tectonic sources that may contribute to the raw time series include coseismic offsets, post-seismic deformation, and/or aseismic transients.

[13] The only significant earthquake that occurred in this region was the 1992 M_w = 7.7 Nicaragua tsunami earthquake; however, *Norabuena et al.* [2004] showed that this event likely accounted for <2 mm/yr post-seismic deformation in Nicoya by 1997. Given our observation period from 1996 to 2010, the post-seismic response induced by the 1992 event was likely on the order of velocity uncertainty, thus not large enough to be considered as a signal source.

[14] Six slow-slip episodes were observed near Nicoya with an average recurrence interval of 21 ± 6 months [*Jiang et al.*, 2012]. The first episode, in early 2000, including three pulses of transient slow-slip propagating at the shallow subduction interface, was suggested by correlated flow rate transients detected across three flowmeters at the frontal prism of the forearc [*Brown et al.*, 2005; *LaBonte et al.*, 2009]. The transient signal was also accompanied with tremor-like noise recorded on collocated ocean bottom seismometers [*Brown et al.*, 2005]. The second episode included two slow-slip transients initiated in May and September 2003, respectively. Both were observed first by three GPS sites on land [*Protti et al.*, 2004] and 2–3 weeks later by a stepwise pressure change in a prism toe borehole ~1 km landward of the trench [*Davis and Villinger*, 2006].

Table 1. GPS Interseismic Velocities Relative to ITRF2005 and the Stable Caribbean Plate[a]

						Relative to ITRF2005 (mm/yr)						Relative to Caribbean (mm/yr)					
Site	Lat (°N)	Lon (°W)	Height (m)	ΔT (yrs)	Days	N	1σ	E	1σ	U	1σ	N	1σ	E	1σ	U	1σ
Nicoya Campaign Sites																	
ACOS	10.5485	84.6024	300.52	14.07	50	11.8	0.3	16.7	0.6	0.1	1.2	4.8	0.5	3.4	0.7	−0.1	1.2
AGUS	9.7241	84.6284	70.55	3.01	8	17.0	1.3	17.4	3.5	6.9	5.9	10.1	1.4	3.7	3.6	6.7	5.9
BAGA	10.5414	85.2612	123.46	10.01	9	21.6	0.5	12.8	1.2	0.1	1.4	15.0	0.7	−0.6	1.3	−0.1	1.4
BALL	10.3834	85.4484	118.18	14.07	9	23.8	0.3	13.6	0.3	0.3	0.9	17.3	0.6	0.2	0.5	0.0	0.9
BONG	9.7438	85.2069	21.40	10.04	11	25.0	0.8	15.6	0.8	−4.5	2.0	18.4	0.9	1.9	0.9	−4.7	2.0
CABU	10.1358	84.7756	499.18	7.26	10	16.6	1.0	12.3	1.0	0.4	2.5	9.7	1.1	−1.3	1.1	0.2	2.5
CEBA	10.2491	85.7761	90.32	10.06	11	21.3	0.5	13.7	0.7	−4.0	1.8	14.8	0.7	0.2	0.8	−4.2	1.8
CORO	9.8630	85.3696	98.86	3.00	7	29.0	0.6	12.4	3.4	1.2	5.9	22.3	0.7	−1.2	3.4	1.0	5.9
CRUZ	11.0543	85.6337	267.23	14.11	13	16.2	1.0	6.8	0.7	−0.3	1.6	9.7	1.1	−6.3	0.8	−0.5	1.6
DIRI	10.2718	85.6106	82.04	10.06	13	24.5	0.3	13.8	0.8	−0.2	1.8	17.9	0.5	0.4	0.9	−0.5	1.8
GRAN	10.5622	85.6530	122.36	14.09	17	20.8	0.3	11.0	0.4	−1.7	0.9	14.3	0.6	−2.3	0.5	−2.0	0.9
GUAR	10.1400	85.4497	135.44	7.04	6	26.1	0.3	15.1	1.5	−6.8	2.0	19.5	0.6	1.6	1.5	−7.0	2.0
GUIO	9.9231	85.6585	31.18	10.02	10	29.9	0.5	22.6	0.6	−9.6	1.1	23.4	0.7	9.0	0.7	−9.9	1.1
HOJA	10.0795	85.3824	240.98	10.05	13	25.8	0.2	16.9	1.2	0.1	1.2	19.2	0.5	3.3	1.3	−0.2	1.2
JICA	9.9751	85.1360	61.45	14.07	14	21.6	0.3	15.5	0.4	−1.2	0.9	14.9	0.5	1.9	0.6	−1.4	0.9
LEON	9.9365	85.1868	276.88	10.00	9	22.4	0.4	16.1	0.7	−3.4	1.6	15.7	0.6	2.5	0.8	−3.6	1.6
LOCA	9.6701	85.0742	157.60	3.02	7	21.0	1.4	21.4	2.4	−1.9	3.8	14.3	1.5	7.7	2.5	−2.2	3.8
MATA	10.3553	85.8129	77.80	14.06	17	20.1	0.3	11.3	0.9	−3.6	1.1	13.7	0.5	−2.1	1.0	−3.8	1.1
PALO	10.2415	85.2203	40.19	10.03	10	22.2	0.6	14.8	0.5	−4.2	1.6	15.5	0.8	1.4	0.6	−4.4	1.6
PAQU	9.8322	84.9551	80.31	14.08	13	22.1	0.4	15.1	0.5	−2.4	1.4	15.4	0.6	1.4	0.6	−2.7	1.4
POTR	10.8474	85.5691	155.80	10.05	15	18.6	0.6	9.2	1.4	0.2	1.7	12.1	0.7	−4.0	1.5	0.0	1.7
SAMA	9.8892	85.5488	45.57	14.05	11	31.8	0.4	18.7	0.6	−10.6	0.9	25.3	0.6	5.1	0.7	−10.8	0.9
SJOS	10.3656	84.9482	1062.24	14.10	12	19.0	0.4	13.5	0.5	0.1	1.2	12.3	0.6	0.1	0.6	−0.1	1.2
SJUA	10.0632	85.7569	44.36	14.06	13	24.6	0.5	18.5	0.8	−7.7	1.1	18.1	0.6	4.9	0.9	−8.0	1.1
TENO	10.6018	85.0983	373.45	10.05	10	20.0	0.6	11.5	1.2	−1.6	2.1	13.3	0.8	−1.8	1.3	−1.8	2.1
VENA	10.1611	85.7917	24.76	10.03	11	22.1	0.5	15.7	0.9	−5.3	1.6	15.6	0.7	2.2	1.0	−5.5	1.6
Nicoya Continuous Sites																	
BIJA	9.7500	84.5769	555.63	0.80	294	20.8	3.6	17.3	2.9	12.8	9.2	13.9	3.6	3.6	2.9	12.5	9.2
BON2	9.7645	85.2025	27.97	5.32	1702	22.6	0.6	14.7	0.6	−4.6	1.5	15.9	0.8	1.0	0.7	−4.8	1.5
CABA	10.2379	85.3435	26.96	0.96	353	27.4	2.3	20.2	1.9	3.2	7.8	20.8	2.4	6.7	1.9	3.0	7.8
EPZA	10.1409	85.5681	668.40	0.96	323	31.0	2.5	21.4	2.0	4.3	7.3	24.4	2.6	7.9	2.0	4.1	7.3
GRZA	9.9155	85.6356	39.32	4.25	1201	30.4	0.8	20.6	0.7	−11.2	1.8	23.9	0.9	6.9	0.8	−11.4	1.8
HATI	10.2922	85.7101	58.60	4.24	1543	22.4	0.6	13.0	0.6	−3.0	1.8	15.9	0.7	−0.5	0.7	−3.3	1.8
HUA2	10.0177	85.3517	593.92	6.90	2198	24.9	0.3	16.1	0.4	−3.2	1.1	18.3	0.6	2.6	0.6	−3.5	1.1
IND1	9.8646	85.5022	75.29	7.49	2369	31.2	0.4	16.7	0.4	−12.1	1.1	24.6	0.6	3.1	0.6	−12.3	1.1
LAFE	9.8071	84.9603	65.24	1.16	426	28.2	2.0	20.3	1.9	−13.5	7.4	21.4	2.1	6.7	2.0	−13.7	7.4
LEPA	9.9454	85.0312	20.93	4.37	1579	21.3	0.6	14.1	0.7	−0.1	1.9	14.6	0.8	0.5	0.8	−0.3	1.9
LMNL	10.2675	85.0533	102.97	3.33	1216	21.2	0.7	14.3	0.6	0.1	2.4	14.4	0.8	0.8	0.8	−0.1	2.4
PNEG	10.1955	85.8290	19.56	4.39	1501	20.2	0.6	14.1	0.6	−6.7	2.0	13.8	0.8	0.6	0.7	−6.9	2.0
PUJE	10.1140	85.2725	30.11	6.77	2155	23.6	0.4	16.1	0.4	−2.5	1.1	16.9	0.6	2.6	0.6	−2.8	1.1
PUMO	10.0645	84.9667	17.96	3.16	1141	20.9	0.8	14.0	0.8	1.3	2.5	14.1	0.9	0.5	0.9	1.1	2.5
QSEC	9.8404	85.3573	17.44	4.36	1355	26.4	0.7	13.0	0.7	−4.7	1.8	19.8	0.8	−0.6	0.8	−4.9	1.8
SAJU	10.0671	85.7106	73.44	2.47	903	25.9	1.1	18.1	1.0	−7.0	3.3	19.4	1.2	4.6	1.1	−7.3	3.3
VERA	10.8536	84.8690	64.32	1.13	413	9.9	1.9	17.8	1.7	−2.4	6.8	3.1	2.0	4.6	1.7	−2.7	6.8
Volcano Sites																	
AROL	10.4372	84.7092	754.01	7.86	1251	17.0	0.5	16.0	0.6	−4.3	1.4	10.2	0.6	2.6	0.7	−4.6	1.4
GR38	10.4619	84.7249	677.04	12.26	16	17.0	0.3	19.8	1.1	1.7	1.7	10.2	0.5	6.4	1.2	1.4	1.7
IRZU	9.9669	83.8975	2963.55	3.45	1154	12.9	1.0	14.3	1.3	3.4	3.8	5.7	1.1	0.6	1.4	3.2	3.8
LOLA	10.4901	84.7137	575.83	7.88	828	9.9	0.4	17.4	0.6	−4.5	1.3	3.0	0.6	4.1	0.7	−4.8	1.3
PARK	10.4602	84.7363	583.15	5.25	18	14.7	1.1	21.5	2.0	−1.2	4.2	7.8	1.2	8.1	2.0	−1.4	4.2
WARN	10.4619	84.7209	748.67	12.34	21	17.8	0.4	20.8	0.9	−3.8	2.8	10.9	0.6	7.4	0.9	−4.0	2.8

[a]ITRF2005 is defined by *Altamimi et al.* [2007]. The conversion from ITRF2005 to the Caribbean plate uses the angular velocity and its covariance matrix determined by *DeMets et al.* [2010]. A correction for the translation of Earth's center-of-mass with respect to ITRF2005 is also applied [*DeMets et al.*, 2010]. Abbreviations: Lat, latitude; Lon, longitude; ΔT, observation time span in years; Days, number of data points used; N, north; E, east; U, vertical; 1σ, standard error representing 68% confidence level.

The best-documented episode was the May 2007 slow-slip event detected by the continuous GPS and seismic network in NW Costa Rica [*Outerbridge et al.*, 2010]. The Nicoya continuous GPS network also recorded three other episodes in mid-2005, early-2009, and mid-2011 [*Jiang et al.*, 2012].

[15] In recent interseismic studies, some effort has been spent on removing transient slip signals from time series for continuous sites and modeling corresponding offsets for campaign sites [e.g., *Correa-Mora et al.*, 2008; *Holtkamp and Brudzinski*, 2010]. We chose not to perform this procedure because our major interest lies in determining the long-term strain accumulation, i.e., information that is useful for identifying the total accumulated slip deficit on the subduction interface. Conversely, removing transient slip offsets adds the slip back to the time series increasing the velocity 30–50% [*Correa-Mora et al.*, 2008; *Outerbridge et al.*, 2010]. *Holtkamp and Brudzinski* [2010] showed the difference between interseismic and intertransient rates reflect slip deficit recovered during slow-slip events. Thus, an intertransient coupling result is not warranted for our purposes. We suggest a clarification between "interseismic" and "intertransient" (see Figure 1 of *Correa-Mora et al.* [2008] for an illustration). A proper selection of either depends on whether the focus is megathrust coupling for total strain accumulation contributing to large earthquakes (where the total interseismic coupling is appropriate), or the interface coupling that includes strain energy that is episodically released in transient events (where intertransient coupling is useful).

3. GPS Interseismic Velocities Relative to Caribbean

[16] Interseismic velocities in the Caribbean reference frame (Table 1) are calculated using a CA-ITRF2005 Euler vector (36.9°N, 98.9°W, 0.261°/Ma) and its covariance matrix with adjustment for the translation of Earth's center-of-mass relative to ITRF2005 [*DeMets et al.*, 2010]. The resultant horizontal velocities (Figure 2) indicate distinct behaviors of forearc and non-forearc sites. Non-forearc sites including six volcano sites and two additional sites (ACOS and VERA) NE of the volcanic arc have a relatively small residual with respect to the stable Caribbean plate. Volcano sites may be affected by local deformation, but ACOS and VERA are most likely to be on the stable Caribbean [*Lundgren et al.*, 1999]. On the other hand, the forearc sites located SW of the volcanic arc show an apparent counterclockwise rotation as observed by previous studies [*Lundgren et al.*, 1999; *Iinuma et al.*, 2004; *Norabuena et al.*, 2004; *LaFemina et al.*, 2009]. This motion, we suggest, is the result of forearc sliver motion superimposing on interseismic deformation. To visualize the relative components of the two types of motion, we project horizontal velocities onto local trench-parallel and trench-normal directions.

3.1. Trench-Parallel Velocities

[17] Trench-parallel GPS velocities of the forearc sites show surprising uniformity in its long-term displacement rate, while trench-parallel velocities of the non-forearc sites fall to almost zero (Figure 3a). Taking the general physiographic trend of the trench offshore Nicoya (Figure 7b) as the preferred trench direction (N45°W), the average trench-parallel rate of the forearc sites is about 11 mm/yr, ~1/3 of the trench-parallel component of the plate convergence. The standard error of the weighted average rate is very small (<0.2 mm/yr), but it is calculated on the basis of a predefined trench and hence probably underestimated. To account for the uncertainty in the trench direction, we vary the trench strike by ±5° from N45°W assuming the chance of having the strike outside this range is low. The average rate changes accordingly from 10 to 12 mm/yr, suggesting an uncertainty of ~1 mm/yr.

[18] The rapid rate change from 11 mm/yr to almost zero occurs within a 16 km wide zone between the forearc and non-forearc sites (light cyan shaded zone in Figure 3) in accord with the clustering of frequent strike-slip earthquakes within 20 km of the volcanic arc [*White and Harlow*, 1993]. Compared to interseismic deformation zones of >200 km in some other strike-slip fault systems [e.g., *Lyon-Caen et al.*, 2006; *Schmalzle et al.*, 2006], the observed transition zone in northwestern Costa Rica is surprisingly narrow suggesting a possible shallow locking on the forearc-bounding faults. Presumably most of the shear strain induced by the forearc sliver motion is concentrated close to the Central American volcanic arc. Thus, the northern Costa Rican forearc sliver including area between MAT and the volcanic arc translates as a rigid undeforming block.

[19] After removing the average sliver motion, most residual velocities (Figure 3b) are <2 mm/yr indicating little internal deformation within the northern Costa Rican forearc. However, four coastal sites (gold in Figure 3b) show up to 5 mm/yr deviation from the average. This variation is likely from the strike-slip component of the interseismic strain accumulation, but remains significantly lower than the potential 20 mm/yr strike-slip rate that is missing from the oblique convergence. Therefore, the oblique convergence probably does not contribute significant trench-parallel interseismic strain accumulation at the surface; however, a considerably larger strike-slip motion would be simultaneously released when thrusting occurs on the subduction interface.

[20] The residuals also reveal possible differential forearc motion at the SE end of Nicoya. Three sites (green in Figure 3b) move 3–7 mm/yr slower than others suggesting that a potential transition zone may exist in the entrance of the Nicoya Gulf. We have a detailed discussion on the northern Costa Rican forearc sliver motion separately in another paper (Feng et al., Active deformation near the Nicoya Peninsula, northwestern Costa Rica, between 1996 and 2010: Forearc sliver transport manuscript in preparation, 2012).

3.2. Trench-Normal Velocities

[21] Trench-normal velocities (Figure 4a) are dominated by elastic interseismic strain accumulation of the upper plate resulting from frictional coupling of the subduction interface. Generally, the coastal sites (gold in Figure 4a) show the largest trench-normal velocities indicating the landward projection of the largest coupling offshore. The velocity peak at the elbow of the coastline is coincident with the boundary that separates oceanic crusts generated at the Cocos-Nazca spreading center (CNS) and the East Pacific Rise (EPR) (hereafter referred to as the CNS-EPR boundary) (Figure 1) [*Barckhausen et al.*, 2001]. Overall, the trench-normal velocities decay gradually landward and flatten out

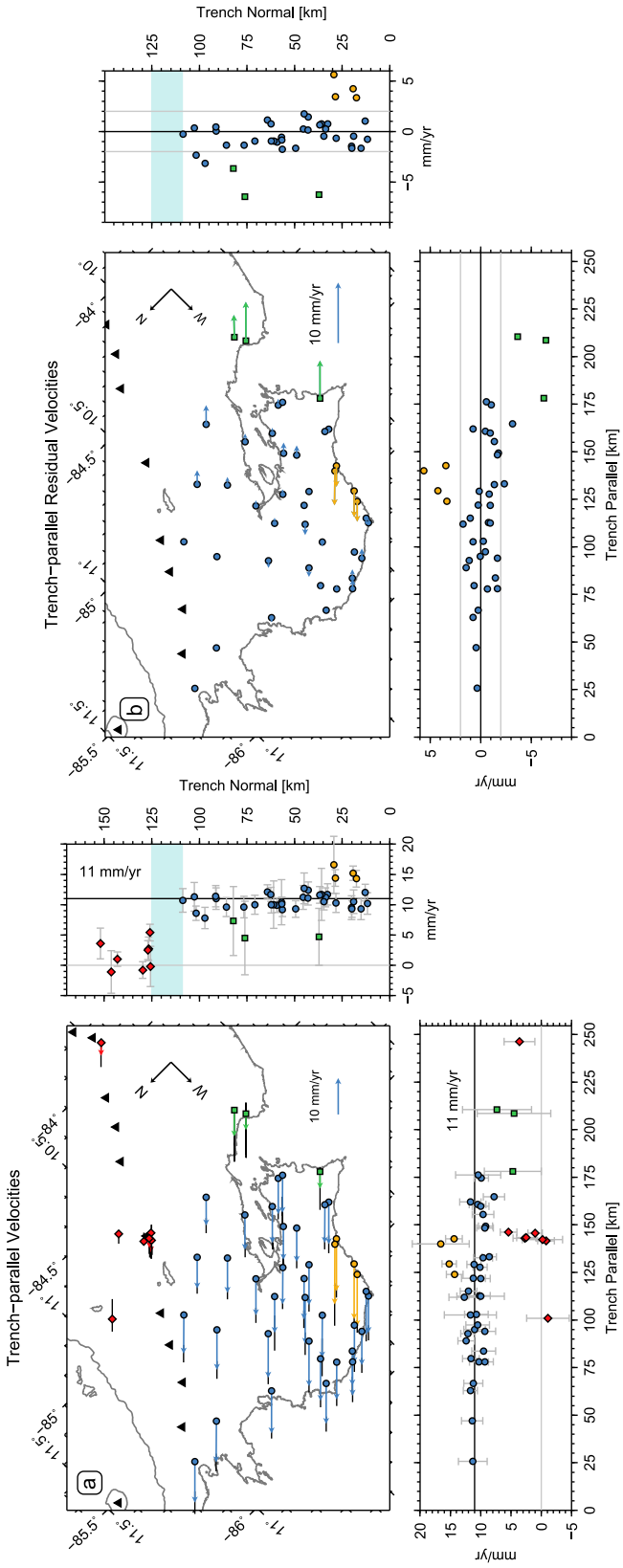

Figure 3. (a) Interseismic trench-parallel velocities from 1996 to 2010 in the Caribbean-fixed frame [*DeMets et al.* 2010] and (b) residuals of the trench-parallel velocities with 11 mm/yr forearc sliver motion removed. For each subplot, bottom panel plots velocities along trench; right panel plots velocities normal to trench with the narrow velocity transition zone highlighted in light cyan. Trench direction is taken as N45°W. Red diamonds, the non-forearc sites; blue circles, the forearc sites; gold circles, the coastal sites, part of the forearc sites; green squares, the sites with large residuals with respect to the northern Costa Rican forearc.

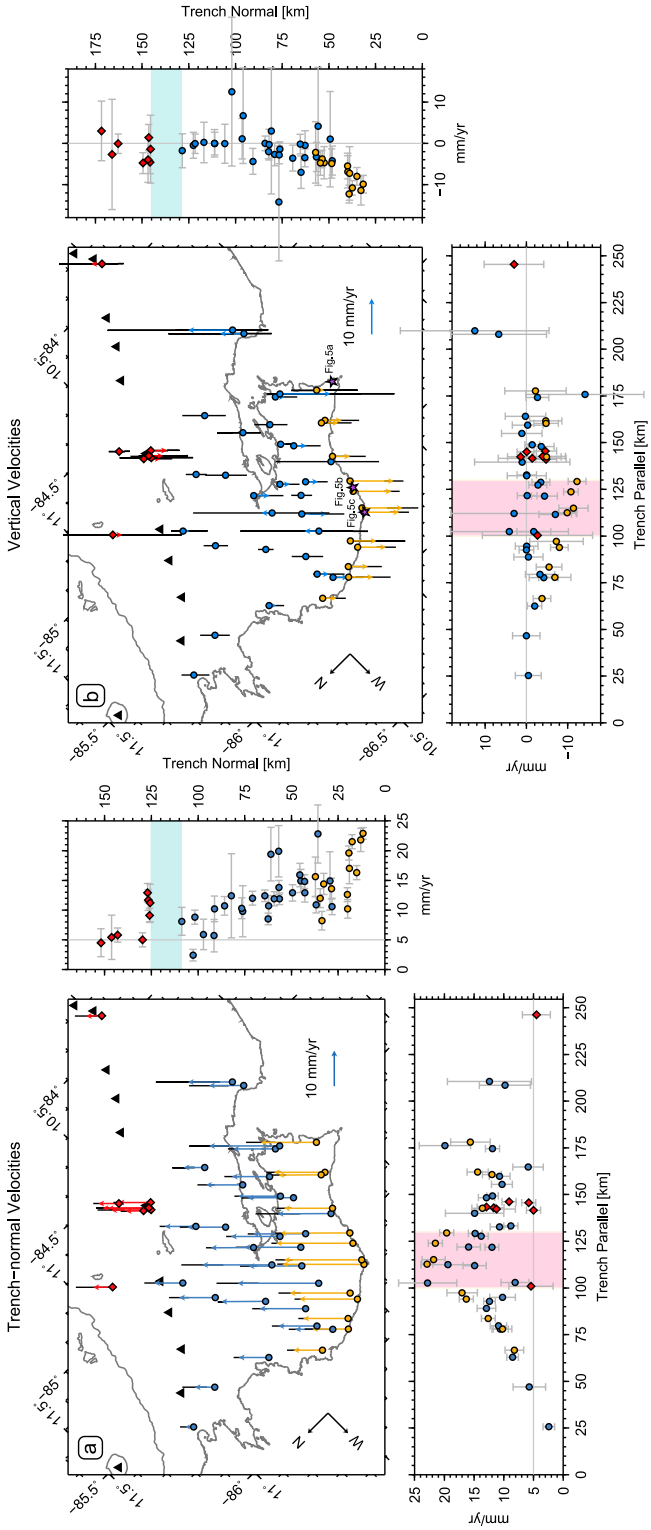

Figure 4. Interseismic (a) trench-normal and (b) vertical velocities from 1996 to 2010 in the Caribbean-fixed frame [*DeMets et al.* 2010]. For each component, bottom panel plots velocities along trench with the velocity peak zone shown in pink; right panel plots velocities normal to trench with the narrow velocity transition zone highlighted in light cyan. Trench direction is taken as N45°W. Red diamonds, the non-forearc sites; blue circles, the forearc sites; gold circles, the coastal sites, part of the forearc sites. Purple stars indicate locations where the pictures in Figure 5 were taken.

Figure 5. Evidence of subsidence at coastal areas. Locations are shown in Figure 4b. (a) Fallen trees caused by coastal subsidence at Cabo Blanco National Park in December 2009. (b) Dead and dying coconut palms on a previously uplifted marine terrace behind the relict of a stone seawall built in the 1990s at West Sámara in June 2008. (c) Eroded fence wall at South Playa Guiones in June 2008. While global mean sea level has risen from 1950 to 2010, on the Pacific side of Costa Rica, it may have actually dropped [*Cazenave and Llovel*, 2010], thus absolute changes in sea level are not expected to be a significant contribution to the observed coastal erosion. The local sea level change is primarily tectonic subsidence, and possibly as large as 0.6 m since 1950 (assuming a subsidence rate of ~10 mm/yr).

at ~5 mm/yr. No obvious difference is apparent across the volcanic arc.

3.3. Vertical Velocities

[22] Similar to trench-normal velocities, vertical velocities (Figure 4b) mainly originate from interseismic strain accumulation. The subsidence rates of the coastal sites (gold sites in Figure 4b) are the largest (>10 mm/yr) indicating a strong coupling offshore. Along trench, the vertical velocities show a 'V' shape with its peak at the CNS-EPR boundary, which is also the point on the coast closest to the trench. We also find clear evidence of subsidence at coastal areas including dead and dying trees, eroded fence walls, and erosion of poles of electric power lines (Figure 5). We do not observe any clear transition from subsidence to uplift. Most remaining sites show essentially zero vertical motion.

3.4. Temporal Variations

[23] To investigate if any temporal variation exists, we divide the observation time from 1996 to 2010 into two 7-yearlong periods that are 1996–2003 and 2003–2010. Because the last campaign before our 2010 campaign was conducted in 2003, the data in 2003 are included in both periods. We subtract the interseismic velocities in 1996–2003 from those in 2003–2010 (Figure 6). The random orientations of the difference vectors do not reveal any consistent pattern, and the differences for most sites are smaller than their errors, hence the temporal resolution of our data is not enough to confidently suggest any temporal variation. However, continuous sites like IND1, HUA2, and PUJE, which have the longest observation time, show more northeastward or eastward motion (>5 mm/yr) in 2003–2010 than in 1996–2003 (red vectors in Figure 6a), which might indicate increasing interseismic coupling with time. Other potential evidence for increased coupling includes more downward motion for most costal sites in 2003–2010 than in 1996–2003 (red vectors in Figure 6b).

4. Interseismic Megathrust Coupling Model

[24] We employ the widely used back slip model proposed by *Savage* [1983] to represent the interseismic strain accumulation induced by coupling on the subduction interface. In the back slip model, virtual "normal" slip on the coupled region indicates slip deficit, i.e., slip less than full plate motion. We assume the interseismic strain accumulation is purely elastic and will be presumably released in future large earthquakes with negligible permanent deformation in the upper plate.

4.1. Model Input Data

[25] As discussed in section 3.1, the horizontal signals from the interseismic strain accumulation are dominated by the trench-normal component with little contribution from the trench-parallel component. Therefore, we use only the trench-normal and vertical velocities to invert for slip distribution across the subduction interface. Although vertical uncertainties are 2–3 times larger than horizontal uncertainties, vertical velocities are well suited for constraining the downdip limit of the locking zone [*Lundgren et al.*, 1999]. Moreover, the fifteen years' observation allows us to obtain relatively reliable vertical measurements for the first time in northern Costa Rica, and thus the vertical data are included in the modeling as well.

4.2. Model Geometry

[26] The 2-D geometry of the plate interface is derived from the well-located plate interface and slab seismicity [*Ghosh et al.*, 2008] using the maximum seismicity method [*Thomas et al.*, 2007]. Although steepening of the plate interface from CNS to EPR has been observed along strike above ~20 km depth [*DeShon et al.*, 2006], we simplify the interface using planar row segments that have an increasing dip with depth as a first order approximation. To construct a representative 2-D cross section perpendicular to the trench from the original seismically defined interface, we use a function that has a constant dip of 11.4° from the trench (4.5 km below sea level) to 18.6 km depth, before steepening as a parabolic function with a maximum dip of 48.1° at

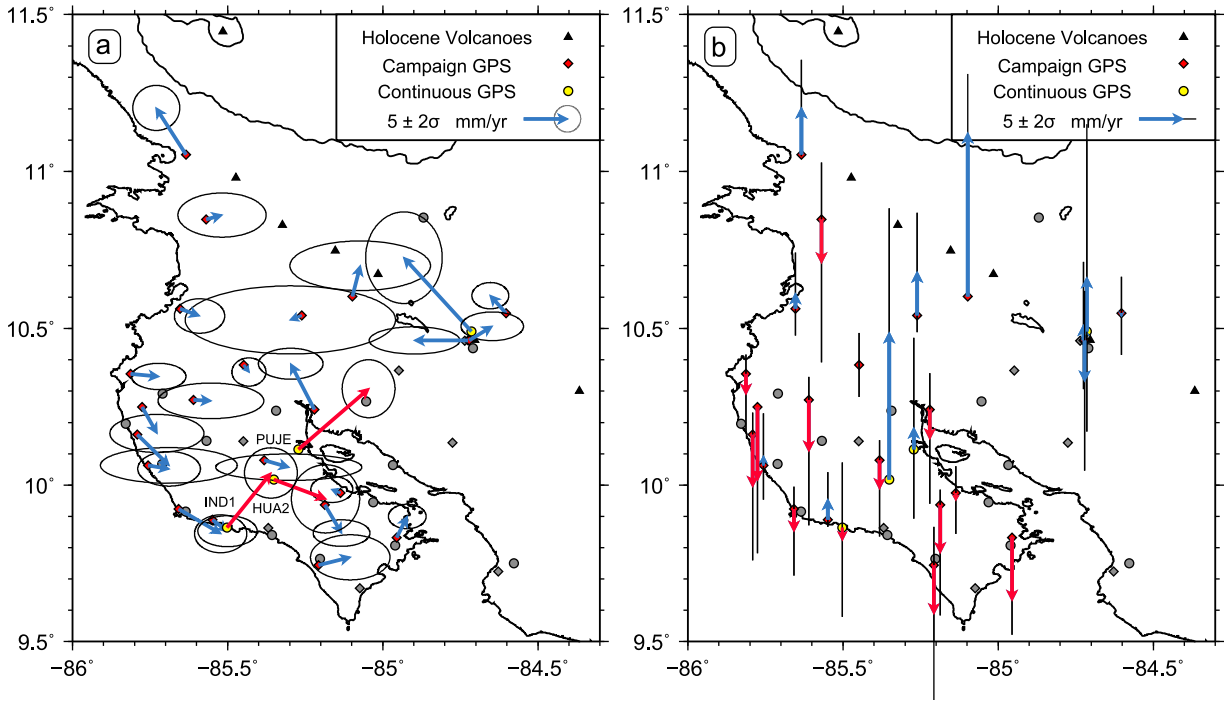

Figure 6. Rate changes in the Caribbean frame between 2003–2010 and 1996–2003 periods from this study. (a) Horizontal rate changes. Continuous sites IND1, HUA2, and PUJE (red vectors) show more northeastward or eastward motion in 2003–2010 than in 1996–2003. (b) Vertical rate changes. Most costal sites (red vectors) show more downward motion in 2003–2010 than in 1996–2003.

62 km depth. The best fit smooth curve is then discretized into planar row segments of ~5 km width to ~60 km depth (Figure 7). As a result, the fault interface is approximated by 30 connected planes with increasing dip at depth. A comparison of our interface with two others by *Norabuena et al.* [2004] and *DeShon et al.* [2006] shows small differences down to ~30 km depth and increasing discrepancies deeper (Figure 7a).

[27] The strike of the interface is fixed at N45°W. Assuming a length of 200 km along strike, the model extends ~40 km more on either side of the Nicoya Peninsula to avoid edge effects. The interface is also discretized into 5-km-wide segments along strike (Figure 7b). The total interface is composed of 30 × 40 rectangular patches.

4.3. Model Formulation and Inversion

[28] Green functions are calculated for the north, east, and vertical displacements of 43 GPS stations (excluding six volcano sites) imposed by unit uniform dip-slip on each patch using the dislocation model of Okada [*Okada*, 1992]. By linear superimposing contributions from each patch, the total observed deformation could be estimated.

[29] Back (normal) slips alone are inverted in the models with their values only allowed to vary between zero and the trench-normal component of the CO-CA convergence at the center of each patch. We refer the ratio of back slip rate to local trench-normal convergence rate as the degree of coupling across the plate interface. A back slip at the trench-normal convergence rate represents full coupling, while a zero back slip indicates freely slipping. The slips at the top boundary of the fault are set to vary freely, while the slips at the bottom and side boundaries are fixed at zero back slip implying freely slipping.

[30] To solve this underdetermined problem with more unknowns (30 × 40 = 1200 patches) than observations (43 × 3 = 129 GPS components), we apply two-dimensional (along strike and dip) second-derivative (Laplacian) smoothing [e.g., *Harris and Segall*, 1987; *Jónsson et al.*, 2002; *Chen et al.*, 2009] to relate adjacent fault slips.

[31] Combining the constraints from data and smoothing, we seek to solve the linear equation system below that relates slips to surface deformation using

$$\begin{bmatrix} w^{-1}d \\ 0 \end{bmatrix} = \begin{bmatrix} w^{-1}G \\ \kappa^2 D \end{bmatrix} m \qquad (1)$$

where d is the observation vector, m is the unknown slip vector, w is the diagonal matrix constructed from observation errors, G is the green function matrix, D is the second-order finite difference operator [*Jónsson et al.*, 2002], κ^2 controls the weight imposed on the smoothing.

[32] The choice of smoothing leads to different model results and no single solution exists. Increasing smoothing always increases model misfit; therefore, we visually inspect the trade-off curve between model misfit and roughness to determine a preferred model [e.g., *Du et al.*, 1992; *Chen et al.*, 2009; *Newman et al.*, 2011]. The root-mean square (RMS) of the weighted-residual sum of squares (WRSS) is used to quantify model misfit, while the average second-order finite difference sum of each patch, is used to represent the degree of smoothing, and is often referred to as the model roughness [*Jónsson et al.*, 2002].

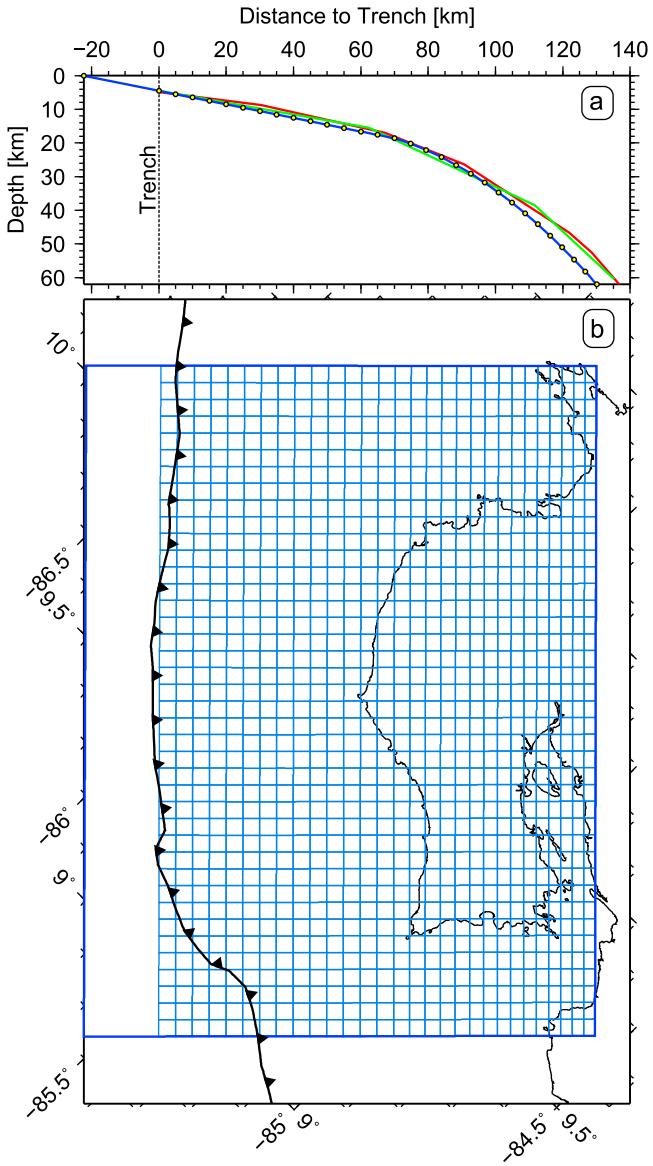

Figure 7. Model geometry. (a) Cross section of the subduction plate interface used in the modeling (blue line) with yellow circles denoting the ends of planar row segments. Green line represents the model interface used by *Norabuena et al.* [2004]. Red line is the generalized subduction interface from Figure 10 in *DeShon et al.* [2006]. Zero depth is at sea level and trench is 4.5 km below sea level. (b) Surface projection of the fault interface and its individual patches.

4.4. Checkerboard Resolution Test

[33] We first conducted a checkerboard resolution test to assess the spatial resolving capability of the Nicoya GPS network on the assumed fault geometry. Because the network has an average station spacing of 15–20 km, which suggests the capability of resolving slips with similar scale, we divided the fault interface into patches of 15 × 20 km^2 area, assigned alternating zero and full convergence back slips to them as a synthetic input (Figure 8a), and calculated the displacements at our stations from this input. Uncertainties of the real data were added to the synthetic displacements before inverting for slips. As expected from the dense coverage, the preferred model at $\kappa = 400$ recovers all the patches beneath Nicoya and other patches within ~30 km distance to the coastline, but loses resolution dramatically toward the trench where no GPS sites exist and at greater depths where fewer sites are available (Figure 8b).

4.5. Model Results

[34] We then ran inversion models using a wide range of smoothing parameters. The preferred model at κ = 15000 (Figure 9b) was chosen because of its location in the inflection corner of the trade-off curve between roughness and misfit (Figure 9d), which introduces substantial smoothing but without the cost of large increasing misfit. For comparison, examples of under-smoothed (Figure 9a) and possibly over-smoothed (Figure 9c) are also provided. We define three types of regions: the fully coupled region with >90% coupling (red), the partially coupled region with ~50% coupling (blue to green), and the freely slipping region with <10% coupling (purple). Because of the reduced resolution toward the boundaries, we only consider the area of high resolution near the coastline as shown by our resolution test (Figure 8).

[35] Independent of the smoothing parameter, high spatial heterogeneity along both strike and dip is pronounced among all three cases. Two fully coupled patches in the Nicoya segment, including one offshore centered at ~15 km depth and the other inland centered at ~24 km depth, are surrounded by freely and partially slipping areas (Figures 9a–9c). This result is different from 50 to 60% coupling found by previous studies [*Norabuena et al.*, 2004; *LaFemina et al.*, 2009]. The overall pattern appears persistent during our interseismic observation, but it is unknown whether it has persisted over many earthquake cycles, as observed in Kamchatka [*Bürgmann et al.*, 2005], Sumatra [*Chlieh et al.*, 2008], and Japan [*Hashimoto et al.*, 2009] from the close correlation of interseismic slip deficit zones with rupture zones of past large earthquakes. In Nicoya, the two fully coupled regions do not seem to resemble either of the 1950 and 1978 rupture regions (Figure 1b). But we note that the rupture regions of the two historic events are not very well determined. Another fully coupled patch SE of the Nicoya Peninsula persists in all three cases (Figures 9a–9c). Although this patch approaches the limit of our high-resolution area, we suspect the coupling of this area is real, particularly because its location coincides with the rupture zone of the 1990 Nicoya Gulf earthquake (Figure 1b).

[36] On the basis of our preferred model (Figure 9b), the geodetic moment accumulation rate of the Nicoya segment is calculated to be 9.0 × 10^{18} N m/yr using rigidity = 30 GPa. Assuming the locking has remained constant, the Nicoya segment has accumulated enough strain between 1950 and 2010 to generate an M_w 7.8 1950-type earthquake. Continued monitoring of the Nicoya seismic gap is highly recommended considering the potential of seismic failure along the interseismic strong-coupling patches [e.g., *Hashimoto et al.*, 2009; *Moreno et al.*, 2010].

5. Discussion

[37] The unprecedented image of interseismic coupling along the shallow subduction megathrust between 1996 and

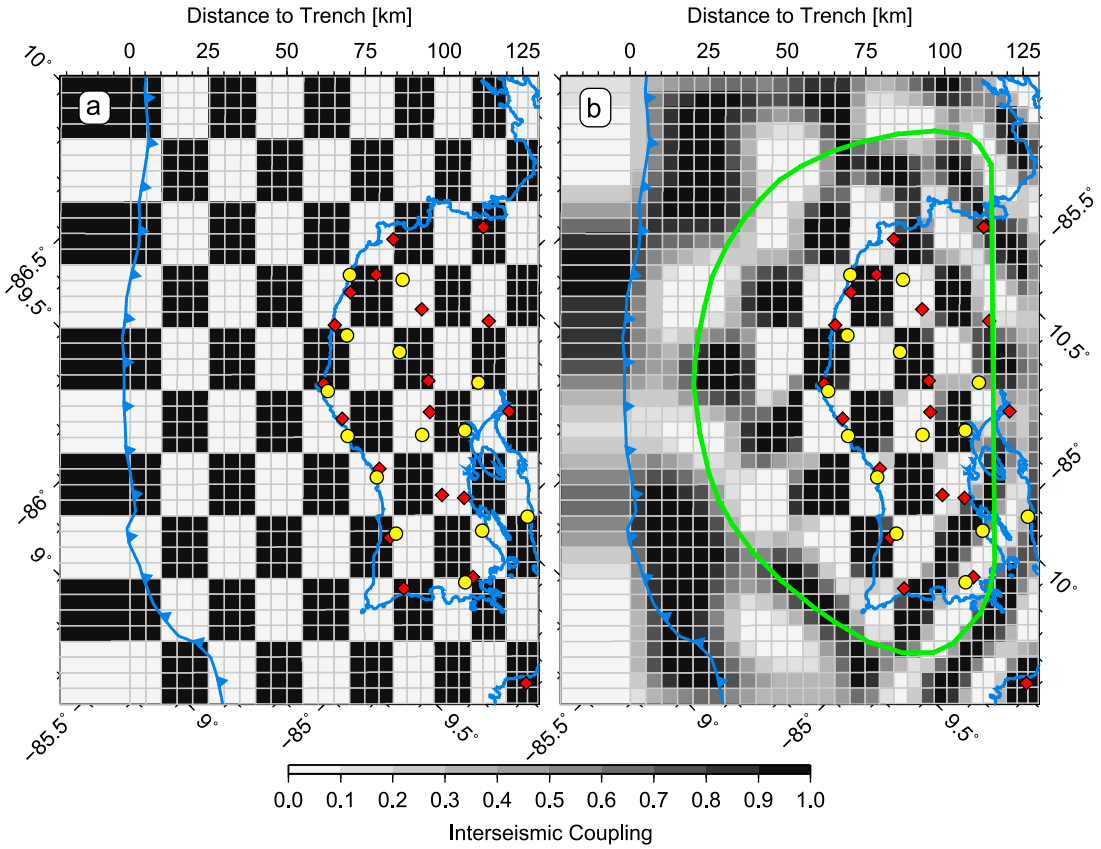

Figure 8. Checkerboard test on the spatial resolution of the dense Nicoya GPS network. (a) Synthetic input slip distribution used to create a synthetic deformation field. (b) Output best fit slip distribution at $\kappa = 400$ inverted from the synthetic surface deformation. Green line outlines the area with high resolution. Red diamonds, the campaign sites; yellow circles, the continuous sites.

2010 allows us to compare long-term locking with short-term features including microearthquakes, low-frequency earthquakes (LFEs), non-volcanic tremor (NVT), and slow-slip events (SSE) (Figure 10).

5.1. Correlation Between Interface Microseismicity and Partially Coupled Regions

[38] Most strikingly, the interface seismicity between late-1999 and mid-2001 [*Ghosh et al.*, 2008] is concentrated in the partially coupled region between the two fully coupled regions forming a narrow band. On the EPR side, the correlation between microseismicity and partial coupling is particularly strong, while on the CNS side some microearthquakes appear in the fully coupled area, which may reflect temporal change in coupling or an artifact due to our planar interface geometry. Microearthquakes are almost absent within the shallow full-coupling zone (a region that was instrumented with 14 ocean bottom seismometers during the 1999–2001 observation) and slightly more occur within the deep full-coupling zone. On the contrary, microseismicity is dominant in the partial-coupling zones, and may reflect a transition in effective normal stress that weakens the plate interface and allows intermediate creep [*Schwartz and DeShon*, 2007]. *Schwartz and DeShon* [2007] suggested that plate interface microseismicity correlates with the 250°C isotherm line where the onset of basalt dehydration and/or permeability reduction may potentially increase pore pressure and reduce effective normal stress. On the other hand, the location of the microseismicity coincides with the bending of the subducting plate where dip increases rapidly (Figure 10a). In the EPR-generated crust, we suspect the normal-faulting, apparent within the subducting slab [*von Huene et al.*, 2000; *Ranero and von Huene*, 2000; *Ranero et al.*, 2003], may release more fluid at the sharp downward bend where the slab is flexed, as was suggested from slab fluid input variations in arc lavas [*Patino et al.*, 2000]. Further north, in Nicaragua, where bending-related faulting is dominant, the strongest fluid signals were found in western Nicaragua where lower-plate fractures are the most pervasive [*Patino et al.*, 2000]. Overall, our results confirm that interseismic microseismicity neither defines the strong-coupling patches nor marks the updip or downdip limit of the seismogenic zone in Nicoya [*Newman et al.*, 2002; *Norabuena et al.*, 2004; *DeShon et al.*, 2006; *Schwartz and DeShon*, 2007].

5.2. Along-Strike Variations in Coupling

[39] Along strike, a 5-km upward and seaward shift in the updip limit of interface seismicity has been identified to occur at the transition from EPR to CNS [*Newman et al.*, 2002; *DeShon et al.*, 2006], which was associated with the thermal difference between the anomalously cold EPR crust due to hydrothermal circulation and the normal CNS crust

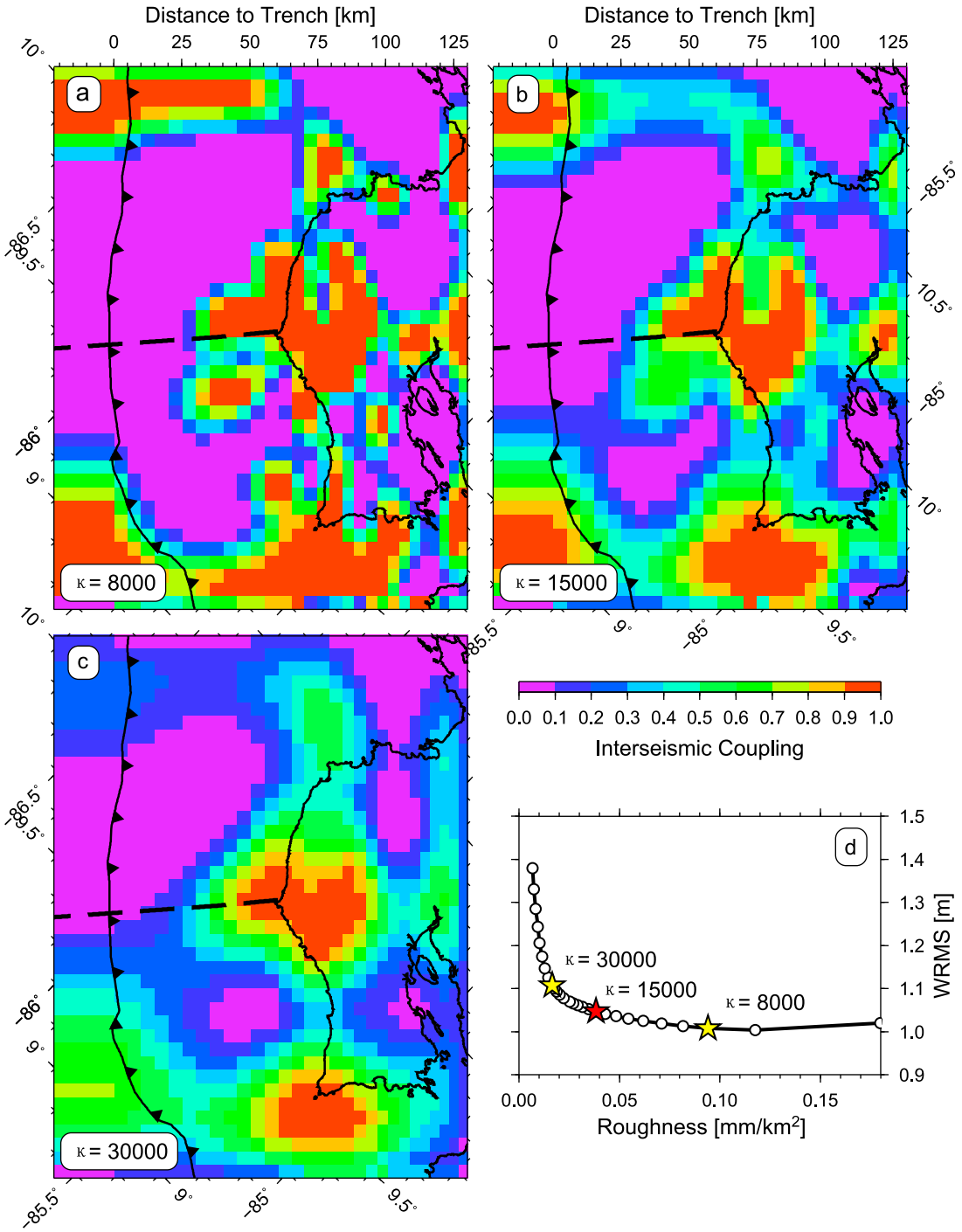

Figure 9. Surface projection of interseismic coupling distribution of the best fit models for selected values of the smoothing parameter κ: (a) κ = 8000, (b) κ = 15,000, and (c) κ = 30,000. As smoothing increases, slip becomes more distributed. (d) Trade-off curve between decreased roughness (increased smoothing) and increased WRMS misfit. Our preferred model at κ = 15000 is chosen in the inflection corner of the curve.

cooled only by conduction [*Fisher et al.*, 2003]. Interestingly, we identify a similar upward and seaward along-strike change in the coupled region crossing the CNS-EPR boundary as mimicked by the seaward shift of the 100°C and 150°C isotherm lines (Figure 10b).

5.3. Updip Transition in Coupling

[40] The updip limit of the seismogenic zone defined by the shallow locked patch is located at ~10 km depth and is ~25 km landward from MAT, similar to what was previously suggested by *Norabuena et al.* [2004] (Figure 10b). The correspondence of the 100–150°C isotherm to the updip limit of the seismogenic zone has been shown in many other subduction zones including south Alaska, Cascadia, Chile, and SW Japan [e.g., *Oleskevich et al.*, 1999; *Spinelli and Saffer*, 2004]. In this temperature range, water contained in sediments that enter subduction zones is released by diagenetic and low-grade metamorphic processes (e.g., opal to quartz and smectite to illite) and expelled by compaction and consolidation [*Moore and Saffer*, 2001]. *Spinelli and Saffer* [2004] proposed that the dewatering processes could decrease fluid pressure, increase effective normal stress and thus may control the transition from aseismic stable sliding to coseismic stick-slip at shallow depths of the Nicoya subduction zone. The estimated maximum depth of the 100°C isotherm is slightly updip of the microseismicity [*Harris et al.*, 2010] and within the shallow fully coupled patch. Considering the uncertainties (~20–30 km) associated with model assumptions [*Harris et al.*, 2010], the 100°C isotherm roughly corresponds to the updip limit of the seismogenic zone.

5.4. Downdip Transition in Coupling

[41] The downdip region of the deep fully coupled patch from our preferred model is located at 28–29 km depth (Figure 10). A very narrow partially coupled transition region may exist between the fully coupled region and the continental Moho. The downdip limit of the seismogenic zone has been suggested to be controlled by either the 350°C isotherm or the serpentinized mantle wedge depending on which the subducting plate encounters first [*Hyndman et al.*, 1997; *Oleskevich et al.*, 1999]. Beneath Nicoya, the oceanic slab intersects the continental Moho at 30–35 km depth (Figure 10) with the mantle wedge 15–25% serpentinized [*DeShon and Schwartz*, 2004; *DeShon et al.*, 2006]; however, the intersection of the 350°C isotherm with the subduction interface varies according to different thermal models, which makes it difficult to determine the controlling factor for the downdip limit [*DeShon et al.*, 2006; *Harris et al.*, 2010]. Cooler thermal models without frictional heating suggest the intersection of 350°C isotherm with the subducting plate is well below the mantle wedge, while

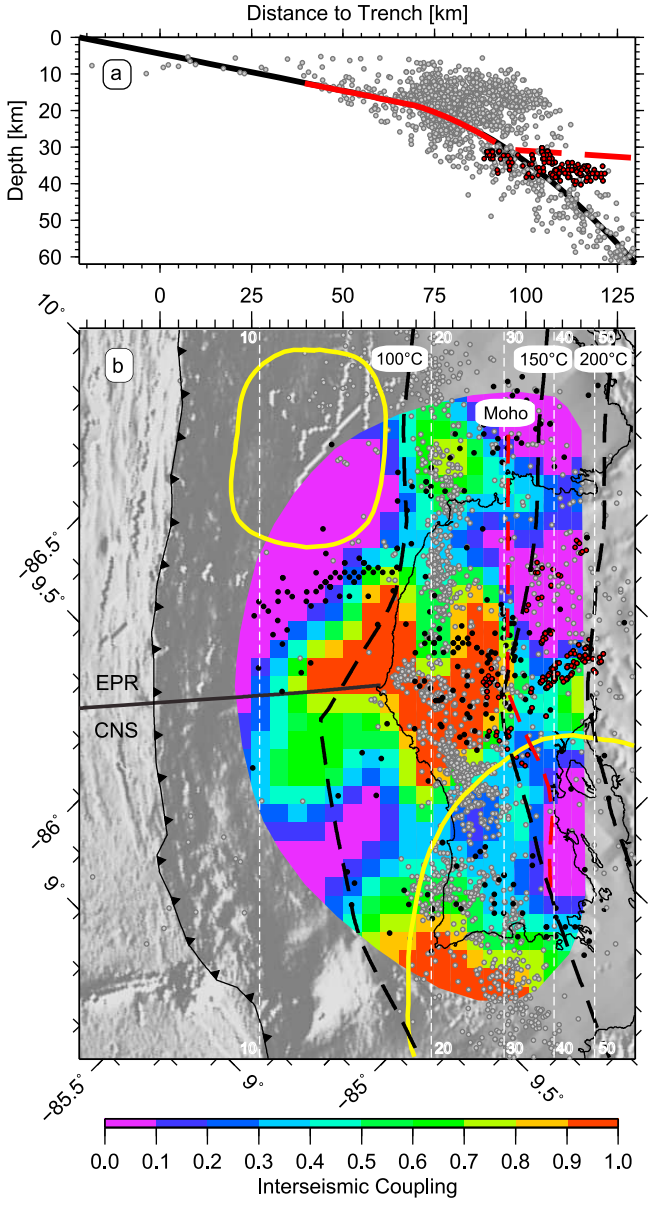

Figure 10. Comparison of our preferred model at κ = 15,000 with interplate microearthquakes, NVT, LFEs, SSE and isotherms. (a) Cross section of the subduction plate interface with the fully locked (>90%) portion in red. Red dash line is the continental Moho inferred from the tomography study by *DeShon et al.* [2006]. Gray circles are interface seismicity between late-1999 and mid-2001 taken from *Ghosh et al.* [2008]. Red circles are LFEs located by *Brown et al.* [2009]. (b) Surface projection of the interseismic coupling distribution of our preferred model. Only high resolution part determined by the checkerboard test is plotted. Thin white dash lines are depth contours derived from our 2-D profile with a contour interval of 10 km. Thick black solid line is the CNS-EPR boundary and its landward projection [*Barckhausen et al.*, 2001]. Red dash line is the continental Moho [*DeShon et al.*, 2006; *Schwartz and DeShon*, 2007]. Thick black dash lines are 100°C, 150°C, and 200°C isotherms that represent a maximum depth without considering frictional heating along the plate interface [*Harris et al.*, 2010]. Note the isotherms could shift seaward depending on models. Yellow curves outline updip and downdip slip patches of the 2007 SSE determined by *Outerbridge et al.* [2010]. Black dots are tremors from *Outerbridge et al.* [2010] and *Walter et al.* [2011]. The depths of tremors are not well constrained, thus not plotted in Figure 10a. Gray and red circles are the same as described in Figure 10a.

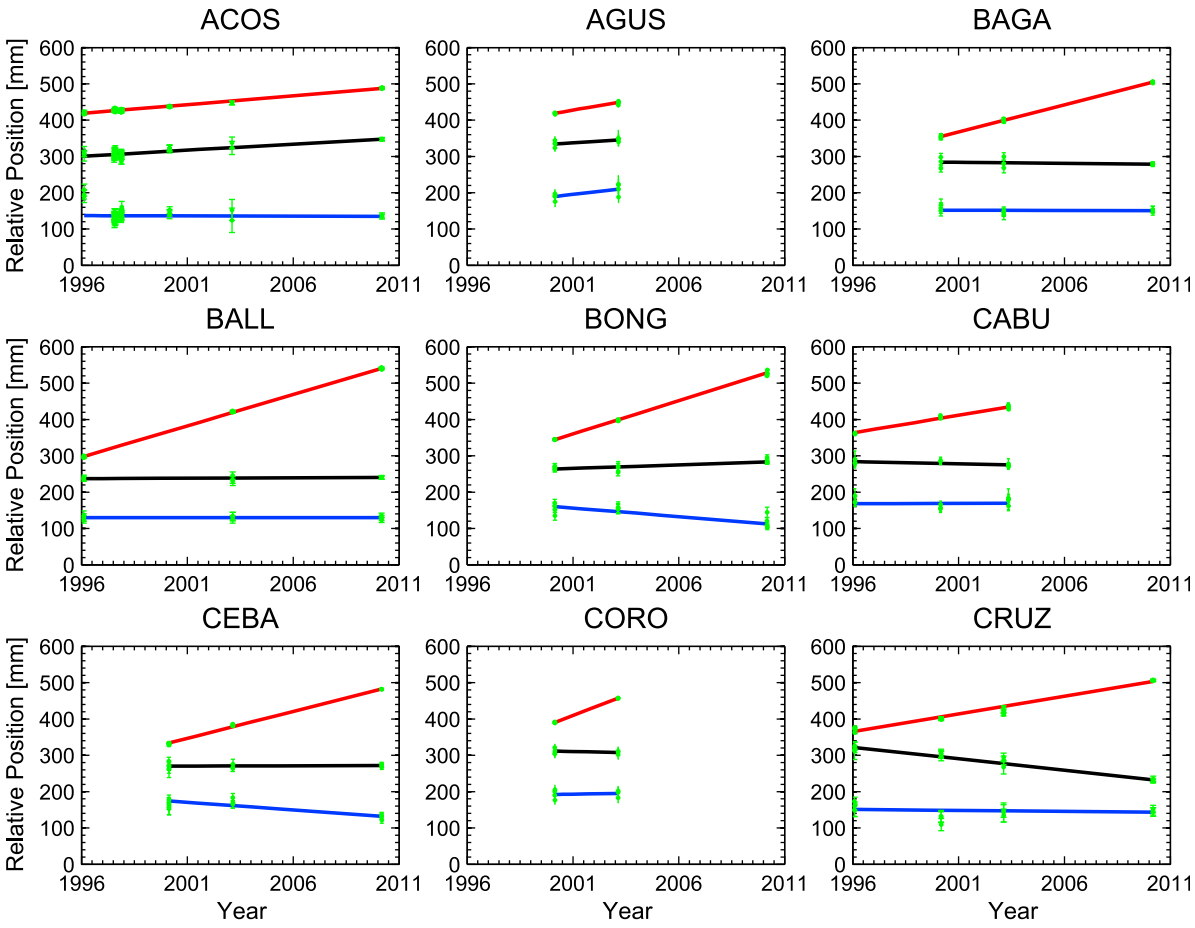

Figure A1. GPS time series relative to the stable Caribbean plate for campaign sites in Nicoya. The components of each station are north (red), east (black), and vertical (blue) from top to bottom. Slope values of best fit lines are given in Table 1.

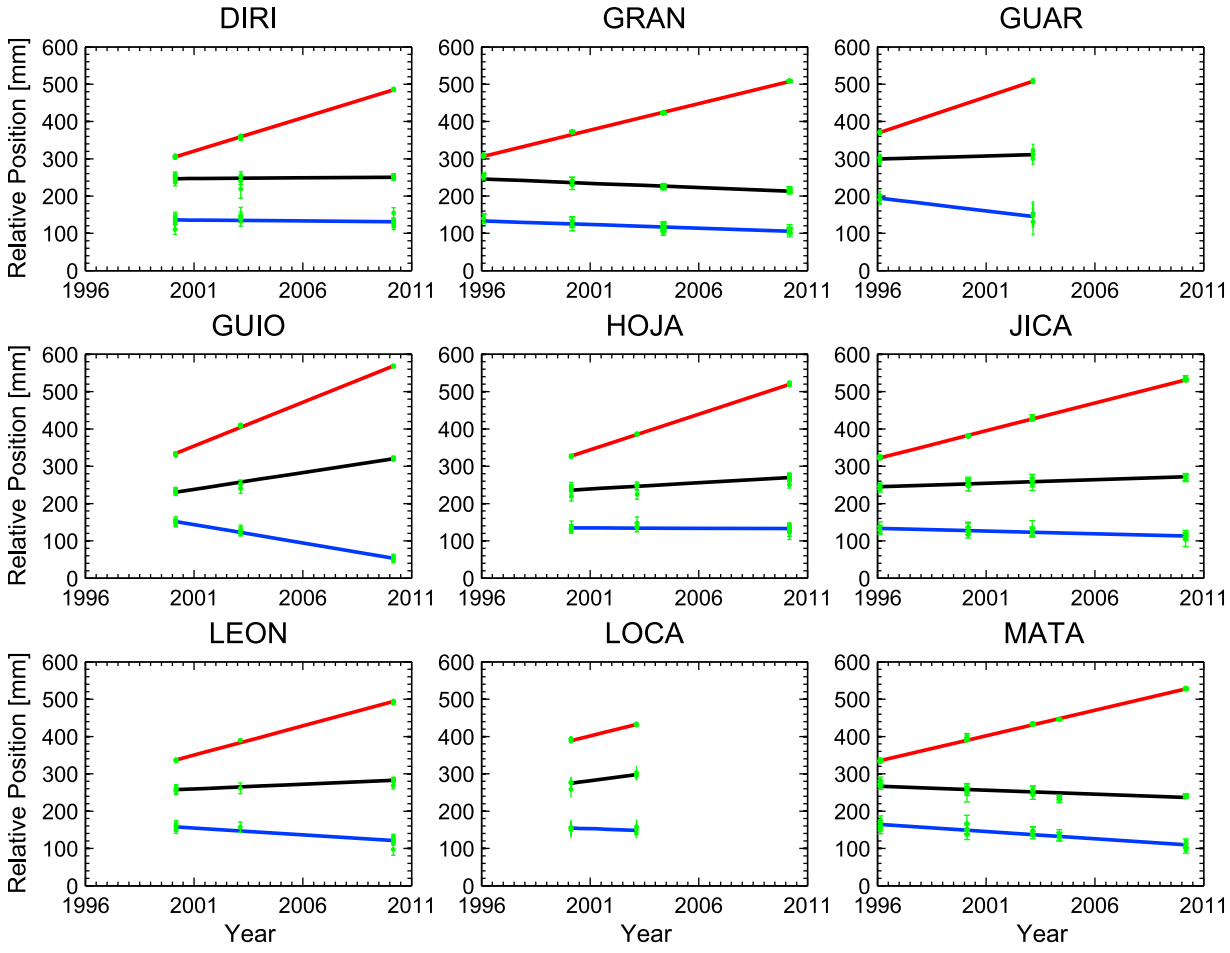

Figure A1. (continued)

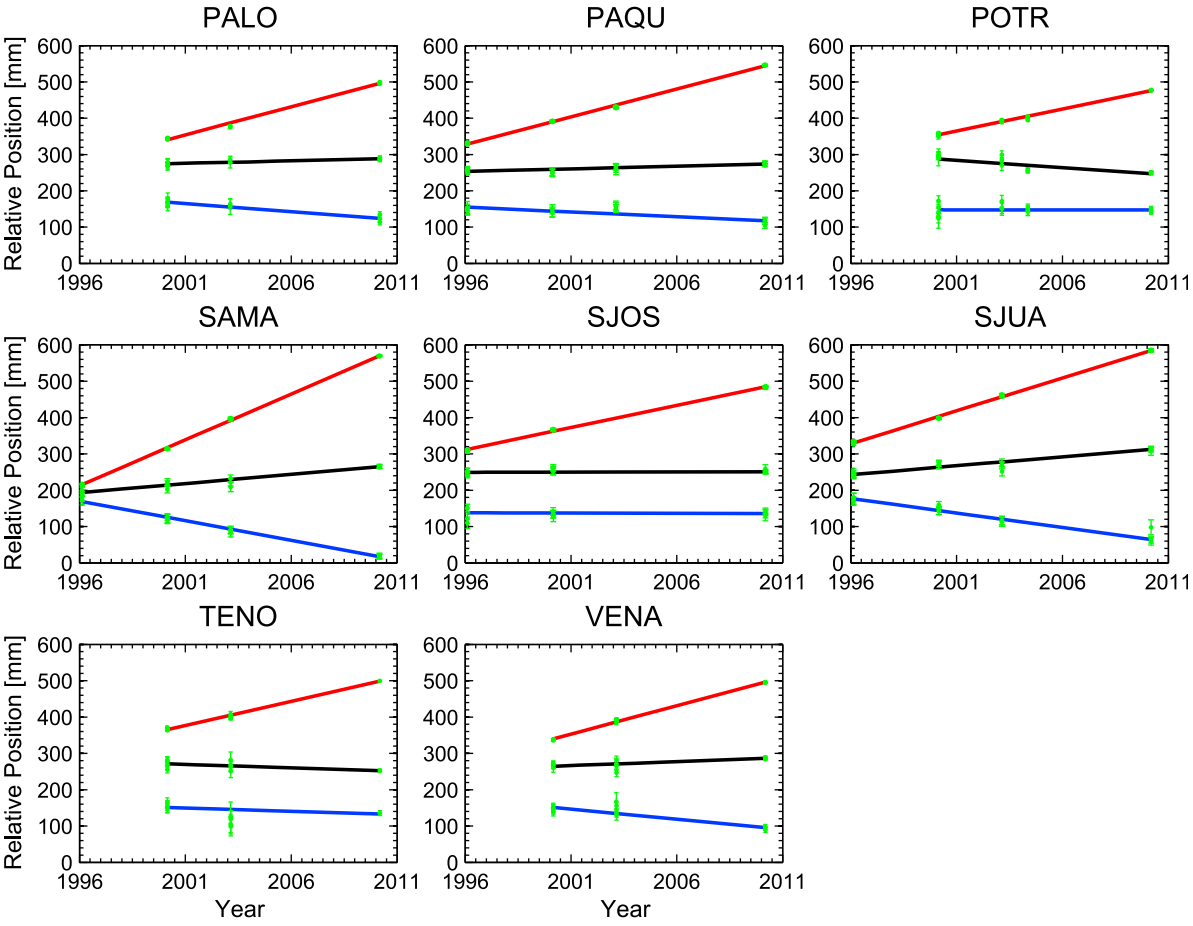

Figure A1. (continued)

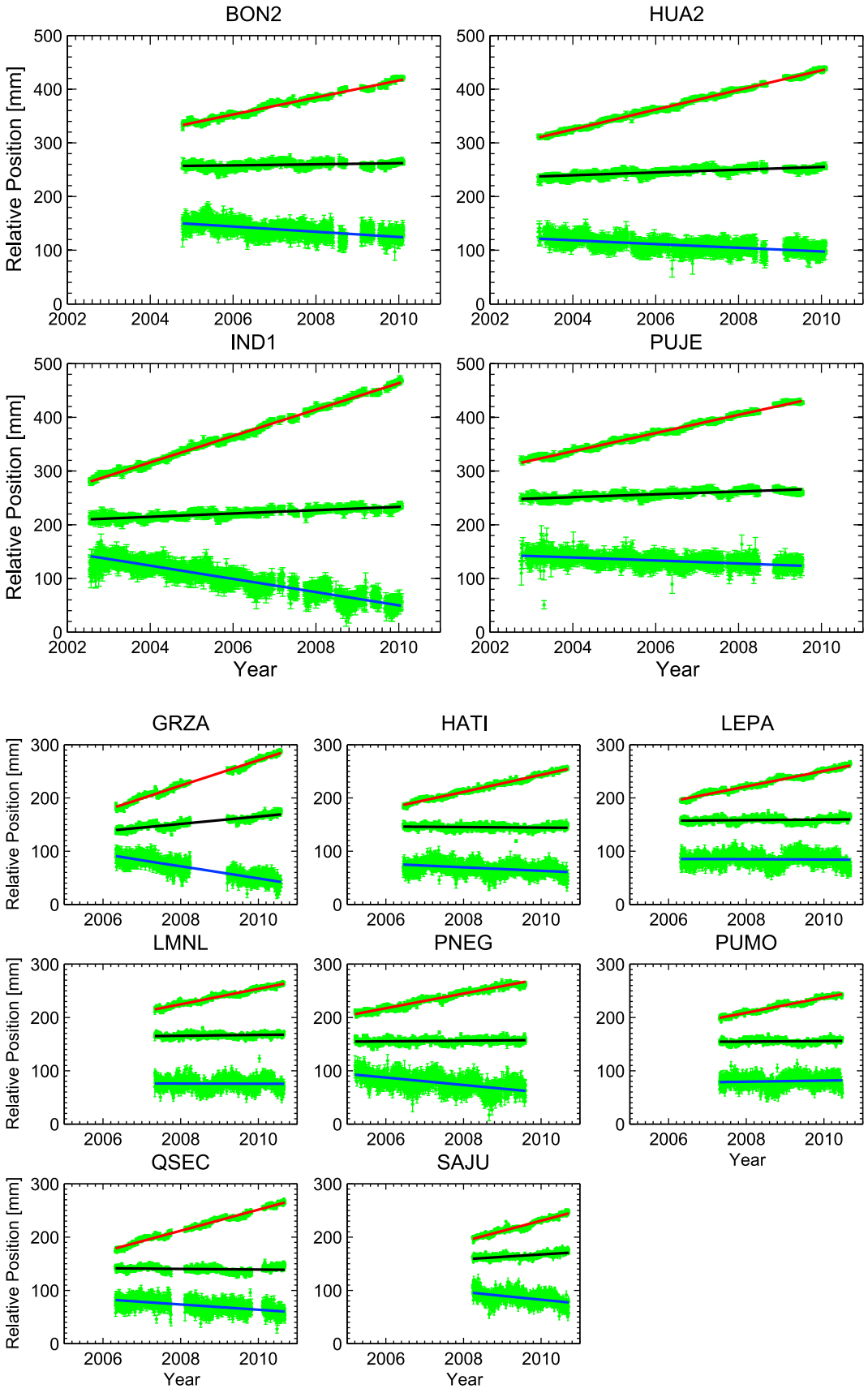

Figure A2. GPS time series relative to the stable Caribbean plate for continuous sites in Nicoya. The components of each station are north (red), east (black), and vertical (blue) from top to bottom. Slope values of best fit lines are given in Table 1.

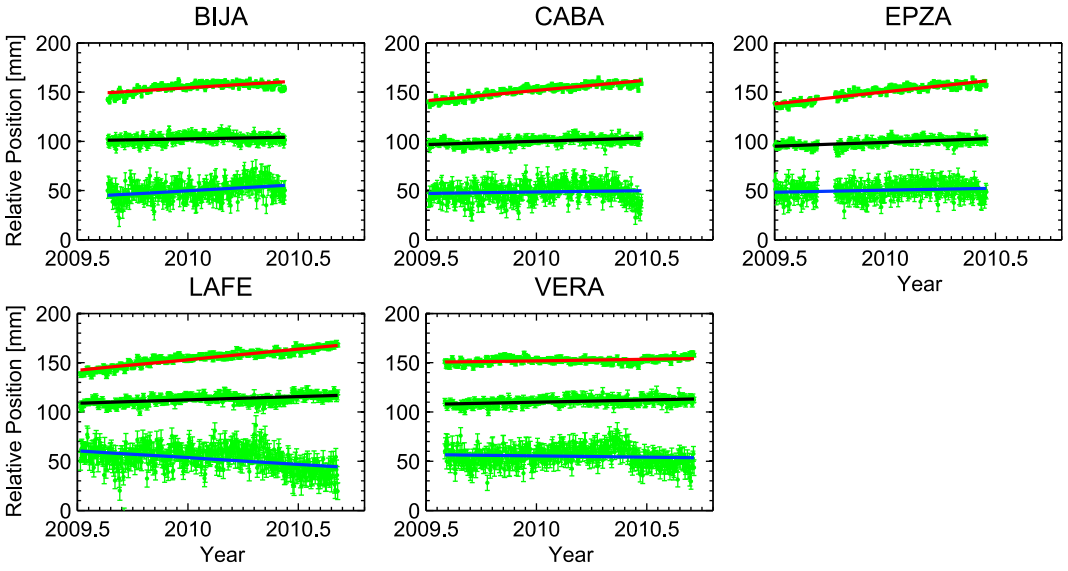

Figure A2. (continued)

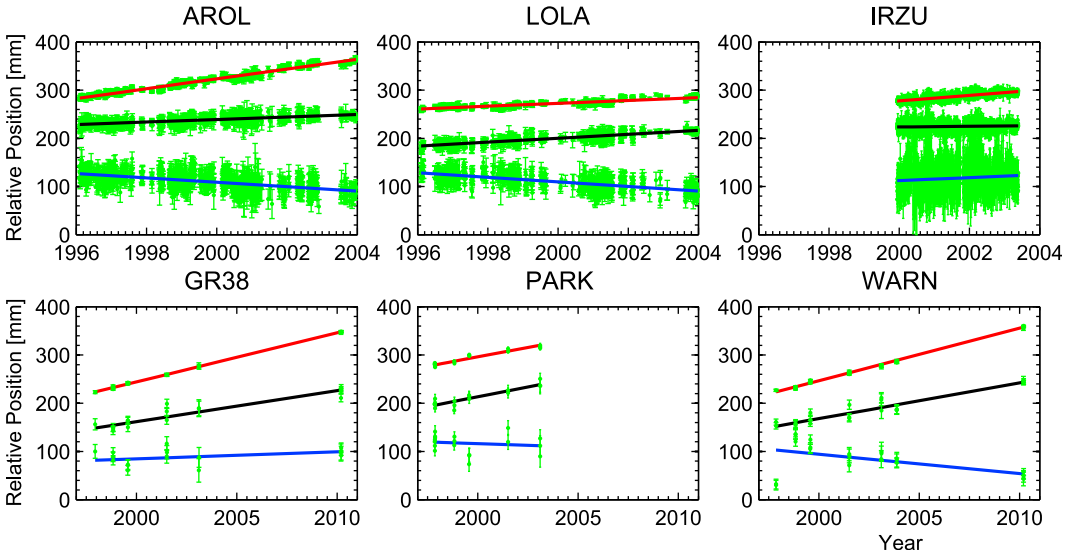

Figure A3. GPS time series relative to the stable Caribbean plate for volcano sites. The components of each station are north (red), east (black), and vertical (blue) from top to bottom. Slope values of best fit lines are given in Table 1.

incorporating frictional heating would bring the 350°C isotherm close to the continental Moho [*Harris et al.*, 2010]. *Harris and Wang* [2002] showed no significant frictional heating is required for Nicoya, therefore the downdip transition from stick-slip to stable sliding at depth is likely not thermally controlled, but related to the serpentinized mantle wedge [*Harris et al.*, 2010].

5.5. Comparison With NVT, LFEs, and SSE

[42] NVT was first discovered in the Nankai subduction zone in SW Japan [*Obara*, 2002] and subsequently observed in other subduction zones from Cascadia [*Rogers and Dragert*, 2003], Costa Rica [*Brown et al.*, 2005], Mexico [*Payero et al.*, 2008] to Alaska [*Peterson and Christensen*, 2009]. The NVT waveforms recorded in SW Japan, northern Cascadia, and northern Costa Rica contain identifiable sequences of LFEs (~1–5 Hz) [*Shelly et al.*, 2007; *Brown et al.*, 2008, 2009; *La Rocca et al.*, 2009, 2010], which suggests that NVT is likely a superposition of bursts of LFEs.

[43] In SW Japan, NVT and LFEs were inferred to be fluid-enabled weak shear slip near the deep interface seismic-aseismic transition zone from precise relocations of LFEs [*Shelly et al.*, 2006; *Brown et al.*, 2009] and focal mechanisms of LFEs [*Ide et al.*, 2007]. In Cascadia, the mechanism is less clear and highly debated. NVT was found distributed over a very wide depth range (>40 km wide) [*Kao et al.*, 2005; *McCausland et al.*, 2005; *La Rocca et al.*, 2008], while newer studies placed NVT near the plate interface [*La Rocca et al.*, 2009, 2010] or well-defined structures [*Kao et al.*, 2009].

[44] In Nicoya, *Walter et al.* [2011] suggested NVT is distributed throughout the seismogenic zone including shallow depths. Interestingly, their shallow locations bound one side of the shallow fully coupled region showing good correlation with the freely slipping region, while the deep tremors between the 100°C isotherm and the continental Moho are more widespread (Figure 10b).

[45] LFEs in Nicoya detected by a network autocorrelation method are clustered at 30–40 km depth [*Brown et al.*, 2009], similar to other subduction zones, with some occurring in the partially coupled transition zone and most others near the tip of the mantle wedge below the Moho (Figure 10). The locations of LFEs in Nicoya approximately correspond to the 150–200°C isotherms, while temperatures for LFEs in SW Japan and Cascadia vary from 325°C to 575°C [*Peacock*, 2009]. The wide range of temperatures for LFEs excludes any dependence on a particular temperature or metamorphic reaction, but indicates the importance of fluid [*Peacock*, 2009].

[46] Seismically detected NVT has been observed to be concurrent both temporally and spatially with geodetically detected transient SSE in SW Japan [e.g., *Obara et al.*, 2004] and Cascadia [e.g., *Rogers and Dragert*, 2003], thus it has been speculated that NVT, LFEs, and SSE are essentially different manifestations of a single process – quasi-static slip [e.g., *Shelly et al.*, 2006; *Wech and Creager*, 2007; *La Rocca et al.*, 2009, 2010; *Peng and Gomberg*, 2010]. However, NVT and long-term SSE observed in the Mexican subduction zone are separated spatially and not completely synchronized in time suggesting different origins for NVT and SSE in Mexico [*Kostoglodov et al.*, 2010]. *Kostoglodov et al.* [2010] proposed that SSE does not produce seismic radiation, but may trigger NVT at favorable locations because of changes in the regional stress field.

[47] In Nicoya, *Outerbridge et al.* [2010] studied the 2007 slow-slip event and found two distinct slip patches: one shallow patch centered at ~6 km depth and one deep patch centered at 25–30 km depth (Figure 10b). Only portions of the two patches are within our high resolution area, but the locations certainly do not overlap the two main fully coupled regions in Nicoya. NVT were found correlated temporally with the 2007 event but not spatially [*Outerbridge et al.*, 2010].

6. Conclusion

[48] The Nicoya Peninsula, within a distance of 60–120 km to the MAT, is an ideal place to study subduction dynamics. Using the campaign and continuous GPS data from 1996 to 2010, we reveal the partial partitioning of the CO-CA plate convergence into 11 ± 1 mm/yr trench-parallel forearc sliver motion and less oblique thrusting on the subduction interface with 20 mm/yr strike-slip motion. Such a partition controls the first-order deformation of NW Costa Rica.

[49] On the basis of our interseismic megathrust coupling model, strong coupling dominates the subduction interface below the Nicoya peninsula, despite that interface microseismicity, NVT, LFEs, and transient slips can occur in the intermediately to weakly coupled regions on the interface. Transient slow-slip events cannot entirely compensate for the slip deficit that has accumulated since the last megathrust earthquake in 1950. A potential M_w 7.8 1950-type earthquake can be expected from the two fully coupled patches of our best fit interseismic megathrust coupling model, one located offshore Nicoya centered at ~15 km depth and the other located inland centered at ~24 km depth. The updip limit of the seismogenic zone is located at ~10 km depth, while the downdip limit of the seismogenic zone is located updip of the continental Moho and likely controlled by the serpentinized mantle wedge. Interface microseismicity neither defines the strong-coupling patches nor marks the updip or downdip limit of the seismogenic zone in Nicoya.

Appendix A: GPS Time Series Relative to the Caribbean Plate

[50] The conversion from raw time series in the ITRF2005 frame to the Caribbean frame uses the angular velocity and its covariance matrix determined by *DeMets et al.* [2010]. A correction for the translation of Earth's center-of-mass with respect to ITRF2005 is also applied [*DeMets et al.*, 2010] (Figures A1–A3).

[51] **Acknowledgments.** This study was supported by the National Science Foundation grant NSF-0847382 to A.V.N. and based on data and equipment services provided by the UNAVCO facility with support from NSF and NASA under EAR-0735156. We greatly appreciate help from Yan Luo in the field. Figures were created using Generic Mapping Tools [*Wessel and Smith*, 1991]. We also thank two anonymous reviewers for their useful reviews.

References

Adamek, S., F. Tajima, and D. Wiens (1987), Seismic rupture associated with subduction of the Cocos ridge, *Tectonics*, *6*(6), 757–774, doi:10.1029/TC006i006p00757.

Altamimi, Z., X. Collilieux, J. Legrand, B. Garayt, and C. Boucher (2007), ITRF2005: A new release of the International Terrestrial Reference Frame based on time series of station positions and Earth Orientation Parameters, *J. Geophys. Res.*, *112*, B09401, doi:10.1029/2007JB004949.

Avants, M., S. Schwartz, A. Newman, and H. DeShon (2001), Large underthrusting earthquakes beneath the Nicoya Peninsula, *Eos Trans. AGU*, *82*(46), Fall Meet. Suppl., Abstract T52E-07.

Barckhausen, U., C. Ranero, R. von Huene, S. Cande, and H. Roeser (2001), Revised tectonic boundaries in the Cocos Plate off Costa Rica: Implications for the segmentation of the convergent margin and for plate tectonic models, *J. Geophys. Res.*, *106*(B9), 19,207–19,220, doi:10.1029/2001JB000238.

Bilek, S. L., S. Y. Schwartz, and H. R. DeShon (2003), Control of seafloor roughness on earthquake rupture behavior, *Geology*, *31*(5), 455–458, doi:10.1130/0091-7613(2003)031<0455:COSROE>2.0.CO;2.

Bilek, S. L., C. E. Elliott, and C. L. Bertelloni (2009), Triggered seismicity associated with the 1990 Nicoya, Costa Rica, M_w = 7.0 earthquake, *Geochem. Geophys. Geosyst.*, *10*, Q04S13, doi:10.1029/2008GC002317.

Brown, J., G. C. Beroza, and D. R. Shelly (2008), An autocorrelation method to detect low frequency earthquakes within tremor, *Geophys. Res. Lett.*, *35*, L16305, doi:10.1029/2008GL034560.

Brown, J. R., G. C. Beroza, S. Ide, K. Ohta, D. R. Shelly, S. Y. Schwartz, W. Rabbel, M. Thorwart, and H. Kao (2009), Deep low-frequency earthquakes in tremor localize to the plate interface in multiple subduction zones, *Geophys. Res. Lett.*, *36*, L19306, doi:10.1029/2009GL040027.

Brown, K. M., M. D. Tryon, H. R. DeShon, L. M. Dorman, and S. Y. Schwartz (2005), Correlated transient fluid pulsing and seismic tremor in the Costa Rica subduction zone, *Earth Planet. Sci. Lett.*, *238*, 189–203, doi:10.1016/j.epsl.2005.06.055.

Bürgmann, R., M. G. Kogan, G. M. Steblov, G. Hilley, V. E. Levin, and E. Apel (2005), Interseismic coupling and asperity distribution along the Kamchatka subduction zone, *J. Geophys. Res.*, *110*, B07405, doi:10.1029/2005JB003648.

Cazenave, A., and W. Llovel (2010), Contemporary sea level rise, *Annu. Rev. Mar. Sci.*, *2*, 145–173, doi:10.1146/annurev-marine-120308-081105.

Chen, T., A. V. Newman, L. Feng, and H. M. Fritz (2009), Slip distribution from the 1 April 2007 Solomon Islands earthquake: A unique image of near-trench rupture, *Geophys. Res. Lett.*, *36*, L16307, doi:10.1029/2009GL039496.

Chlieh, M., J. P. Avouac, K. Sieh, D. H. Natawidjaja, and J. Galetzka (2008), Heterogeneous coupling of the Sumatran megathrust constrained by geodetic and paleogeodetic measurements, *J. Geophys. Res.*, *113*, B05305, doi:10.1029/2007JB004981.

Correa-Mora, F., C. DeMets, E. Cabral-Cano, B. Marquez-Azua, and O. Diaz-Molina (2008), Interplate coupling and transient slip along the subduction interface beneath Oaxaca, Mexico, *Geophys. J. Int.*, *175*(1), 269–290, doi:10.1111/j.1365-246X.2008.03910.x.

Davis, E. E., and H. W. Villinger (2006), Transient formation fluid pressures and temperatures in the Costa Rica forearc prism and subducting oceanic basement: CORK monitoring at ODP sites 1253 and 1255, *Earth Planet. Sci. Lett.*, *245*, 232–244, doi:10.1016/j.epsl.2006.02.042.

DeMets, C., R. G. Gordon, and D. F. Argus (2010), Geologically current plate motions, *Geophys. J. Int.*, *181*, 1–80, doi:10.1111/j.1365-246X.2009.04491.x.

DeShon, H. R., and S. Y. Schwartz (2004), Evidence for serpentinization of the forearc mantle wedge along the Nicoya Peninsula, Costa Rica, *Geophys. Res. Lett.*, *31*, L21611, doi:10.1029/2004GL021179.

DeShon, H. R., S. Y. Schwartz, S. L. Bilek, L. M. Dorman, V. Gonzalez, J. M. Protti, E. R. Flueh, and T. H. Dixon (2003), Seismogenic zone structure of the southern Middle America Trench, Costa Rica, *J. Geophys. Res.*, *108*(B10), 2491, doi:10.1029/2002JB002294.

DeShon, H. R., S. Y. Schwartz, A. V. Newman, V. Gonzalez, J. M. Protti, L. M. Dorman, T. Dixon, D. E. Sampson, and E. R. Flueh (2006), Seismogenic zone structure beneath the Nicoya Peninsula, Costa Rica, from three-dimensional local earthquake P- and S-wave tomography, *Geophys. J. Int.*, *164*, 109–124, doi:10.1111/j.1365-246X.2005.02809.x.

Dixon, T. H., M. Miller, F. Farina, H. Wang, and D. Johnson (2000), Present-day motion of the Sierra Nevada block and some tectonic implications for the Basin and Range province, North American Cordillera, *Tectonics*, *19*(1), 1–24, doi:10.1029/1998TC001088.

Du, Y., A. Aydin, and P. Segall (1992), Comparison of various inversion techniques as applied to the determination of a geophysical deformation model for the 1983 Borah Peak earthquake, *Bull. Seismol. Soc. Am.*, *82*(4), 1840–1866.

Ekström, G., A. M. Dziewonski, N. N. Maternovskaya, and M. Nettles (2005), Global seismicity of 2003: Centroid-moment-tensor solutions for 1087 earthquakes, *Phys. Earth Planet. Inter.*, *148*(2–4), 327–351, doi:10.1016/j.pepi.2004.09.006.

Fisher, A. T., et al. (2003), Abrupt thermal transition reveals hydrothermal boundary and role of seamounts within the Cocos Plate, *Geophys. Res. Lett.*, *30*(11), 1550, doi:10.1029/2002GL016766.

Ghosh, A., A. V. Newman, A. M. Thomas, and G. T. Farmer (2008), Interface locking along the subduction megathrust from *b*-value mapping near Nicoya Peninsula, Costa Rica, *Geophys. Res. Lett.*, *35*, L01301, doi:10.1029/2007GL031617.

Güendel, F. (1986), Seismotectonics of Costa Rica: An analytical view of the southern terminus of the Middle American Trench, PhD dissertation, Univ. of Calif., Santa Cruz.

Harris, R. A., and P. Segall (1987), Detection of a locked zone at depth on the Parkfield, California, segment of the San Andreas fault, *J. Geophys. Res.*, *92*(B8), 7945–7962, doi:10.1029/JB092iB08p07945.

Harris, R. N., and K. Wang (2002), Thermal models of the Middle America Trench at the Nicoya Peninsula, Costa Rica, *Geophys. Res. Lett.*, *29*(21), 2010, doi:10.1029/2002GL015406.

Harris, R. N., G. Spinelli, C. R. Ranero, I. Grevemeyer, H. Villinger, and U. Barckhausen (2010), Thermal regime of the Costa Rican convergent margin: 2. Thermal models of the shallow Middle America subduction zone offshore Costa Rica, *Geochem. Geophys. Geosyst.*, *11*, Q12S29, doi:10.1029/2010GC003273.

Hashimoto, C., A. Noda, T. Sagiya, and M. Matsu'ura (2009), Interplate seismogenic zones along the Kuril-Japan trench inferred from GPS data inversion, *Nat. Geosci.*, *2*, 141–144, doi:10.1038/ngeo421.

Heflin, M., et al. (1992), Global geodesy using GPS without fiducial sites, *Geophys. Res. Lett.*, *19*(2), 131–134, doi:10.1029/91GL02933.

Holtkamp, S., and M. R. Brudzinski (2010), Determination of slow slip episodes and strain accumulation along the Cascadia margin, *J. Geophys. Res.*, *115*, B00A17, doi:10.1029/2008JB006058.

Husen, S., E. Kissling, and R. Quintero (2002), Tomographic evidence for a subducted seamount beneath the Gulf of Nicoya, Costa Rica: The cause of the 1990 M_w = 7.0 Gulf of Nicoya earthquake, *Geophys. Res. Lett.*, *29*(8), 1238, doi:10.1029/2001GL014045.

Hyndman, R. D., M. Yamano, and D. A. Oleskevich (1997), The seismogenic zone of subduction thrust faults, *Isl. Arc*, *6*, 244–260, doi:10.1111/j.1440-1738.1997.tb00175.x.

Ide, S., D. R. Shelly, and G. C. Beroza (2007), The mechanism of deep low frequency earthquakes: Further evidence that deep non-volcanic tremor is generated by shear slip on the plate interface, *Geophys. Res. Lett.*, *34*, L03308, doi:10.1029/2006GL028890.

Ihmlé, P. F. (1996), Monte Carlo slip inversion in the frequency domain: Application to the 1992 Nicaragua Slow Earthquake, *Geophys. Res. Lett.*, *23*(9), 913–916, doi:10.1029/96GL00872.

Iinuma, T., et al. (2004), Inter-plate coupling in the Nicoya Peninsula, Costa Rica, as deduced from a trans-peninsula GPS experiment, *Earth Planet. Sci. Lett.*, *223*, 203–212, doi:10.1016/j.epsl.2004.04.016.

Jiang, Y., S. Wdowinski, T. H. Dixon, M. Hackl, M. Protti, and V. González (2012), Slow slip events in Costa Rica detected by continuous GPS observations, 2002–2011, *Geochem. Geophys. Geosyst.*, *13*, Q04006, doi:10.1029/2012GC004058.

Jónsson, S., H. Zebker, P. Segall, and F. Amelung (2002), Fault slip distribution of the 1999 M_W 7.1 Hector Mine, California earthquake, estimated from satellite radar and GPS measurements, *Bull. Seismol. Soc. Am.*, *92*(4), 1377–1389, doi:10.1785/0120000922.

Kanamori, H., and M. Kikuchi (1993), The 1992 Nicaragua earthquake: A slow tsunami earthquake associated with subducted sediments, *Nature*, *361*, 714–716, doi:10.1038/361714a0.

Kao, H., S.-J. Shan, H. Dragert, G. Rogers, J. F. Cassidy, and K. Ramachandran (2005), A wide depth distribution of seismic tremors along the northern Cascadia margin, *Nature*, *436*, 841–844, doi:10.1038/nature03903.

Kao, H., S.-J. Shan, H. Dragert, and G. Rogers (2009), Northern Cascadia episodic tremor and slip: A decade of tremor observations from 1997 to 2007, *J. Geophys. Res.*, *114*, B00A12, doi:10.1029/2008JB006046.

Kostoglodov, V., A. Husker, N. M. Shapiro, J. S. Payero, M. Campillo, N. Cotte, and R. Clayton (2010), The 2006 slow slip event and nonvolcanic tremor in the Mexican subduction zone, *Geophys. Res. Lett.*, *37*, L24301, doi:10.1029/2010GL045424.

LaBonte, A. L., K. M. Brown, and Y. Fialko (2009), Hydrologic detection and finite element modeling of a slow slip event in the Costa Rica prism toe, *J. Geophys. Res.*, *114*, B00A02, doi:10.1029/2008JB005806.

LaFemina, P., T. H. Dixon, R. Govers, E. Norabuena, H. Turner, A. Saballos, G. Mattioli, M. Protti, and W. Strauch (2009), Fore-arc motion and Cocos Ridge collision in Central America, *Geochem. Geophys. Geosyst.*, *10*, Q05S14, doi:10.1029/2008GC002181.

La Rocca, M., D. Galluzzo, S. Malone, W. McCausland, G. Saccorotti, and E. Del Pezzo (2008), Testing small-aperture array analysis on well-located earthquakes, and application to the location of deep tremor, *Bull. Seismol. Soc. Am.*, *98*(2), 620–635, doi:10.1785/0120060185.

La Rocca, M., K. C. Creager, D. Galluzzo, S. Malone, J. E. Vidale, J. R. Sweet, and A. G. Wech (2009), Cascadia tremor located near plate interface constrained by S minus P wave times, *Science*, *323*, 620–623, doi:10.1126/science.1167112.

La Rocca, M., D. Galluzzo, S. Malone, W. McCausland, and E. Del Pezzo (2010), Array analysis and precise sourcelocation of deep tremor in Cascadia, *J. Geophys. Res.*, *115*, B00A20, doi:10.1029/2008JB006041.

Lonsdale, P. (2005), Creation of the Cocos and Nazca plates by fission of the Farallon plate, *Tectonophysics*, *404*, 237–264, doi:10.1016/j.tecto.2005.05.011.

Lundgren, P., M. Protti, A. Donnellan, M. Heflin, E. Hernandez, and D. Jefferson (1999), Seismic cycle and plate margin deformation in Costa Rica: GPS observations from 1994 to 1997, *J. Geophys. Res.*, *104*(B12), 28,915–28,926, doi:10.1029/1999JB900283.

Lyon-Caen, H., et al. (2006), Kinematics of the North American-Caribbean-Cocos plates in Central America from new GPS measurements across the Polochic-Motagua fault system, *Geophys. Res. Lett.*, *33*, L19309, doi:10.1029/2006GL027694.

MacMillan, I., P. B. Gans, and G. Alvarado (2004), Middle Miocene to present plate tectonic history of the southern Central American Volcanic Arc, *Tectonophysics*, *392*, 325–348, doi:10.1016/j.tecto.2004.04.014.

Mao, A., C. G. A. Harrison, and T. H. Dixon (1999), Noise in GPS coordinate time series, *J. Geophys. Res.*, *104*(B2), 2797–2816, doi:10.1029/1998JB900033.

Marshall, J. S., and R. S. Anderson (1995), Quaternary uplift and seismic cycle deformation, Peninsula de Nicoya, Costa Rica, *Geol. Soc. Am. Bull.*, *107*(4), 463–473, doi:10.1130/0016-7606(1995)107<0463:QUASCD>2.3.CO;2.

Marshall, J., D. Fisher, and T. Gardner (2000), Central Costa Rica deformed belt: Kinematics of diffuse faulting across the western Panama block, *Tectonics*, *19*(3), 468–492, doi:10.1029/1999TC001136.

McCausland, W., S. Malone, and D. Johnson (2005), Temporal and spatial occurrence of deep non-volcanic tremor: From Washington to northern California, *Geophys. Res. Lett.*, *32*, L24311, doi:10.1029/2005GL024349.

Moore, J. C., and D. Saffer (2001), Updip limit of the seismogenic zone beneath the accretionary prism of southwest Japan: An effect of diagenetic to low-grade metamorphic processes and increasing effective stress, *Geology*, *29*(2), 183–186, doi:10.1130/0091-7613(2001)029<0183:ULOTSZ>2.0.CO;2.

Moreno, M., M. Rosenau, and O. Onchen (2010), 2010 Maule earthquake slip correlates with pre-seismic locking of Andean subduction zone, *Nature*, *467*, 198–202, doi:10.1038/nature09349.

Newman, A. V., S. Y. Schwartz, V. González, H. R. DeShon, J. M. Protti, and L. M. Dorman (2002), Along-strike variability in the seismogenic zone below Nicoya Peninsula, Costa Rica, *Geophys. Res. Lett.*, *29*(20), 1977, doi:10.1029/2002GL015409.

Newman, A. V., L. Feng, H. M. Fritz, Z. M. Lifton, N. Kalligeris, and Y. Wei (2011), The energetic 2010 M_w 7.1 Solomon Islands tsunami earthquake, *Geophys. J. Int.*, *186*, 775–781, doi:10.1111/j.1365-246X.2011.05057.x.

Nishenko, S. P. (1991), Circum-Pacific seismic potential: 1989–1999, *Pure Appl. Geophys.*, *135*(2), 169–259, doi:10.1007/BF00880240.

Norabuena, E., et al. (2004), Geodetic and seismic constraints on some seismogenic zone processes in Costa Rica, *J. Geophys. Res.*, *109*, B11403, doi:10.1029/2003JB002931.

Obara, K. (2002), Nonvolcanic deep tremor associated with subduction in southwest Japan, *Science*, *296*, 1679–1681, doi:10.1126/science.1070378.

Obara, K., H. Hirose, F. Yamamizu, and K. Kasahara (2004), Episodic slow slip events accompanied by non-volcanic tremors in southwest Japan subduction zone, *Geophys. Res. Lett.*, *31*, L23602, doi:10.1029/2004GL020848.

Okada, Y. (1992), Internal deformation due to shear and tensile faults in a half-space, *Bull. Seismol. Soc. Am.*, *82*(2), 1018–1040.

Oleskevich, D. A., R. D. Hyndman, and K. Wang (1999), The updip and downdip limits to great subduction earthquakes: Thermal and structural models of Cascadia, south Alaska, SW Japan, and Chile, *J. Geophys. Res.*, *104*(B7), 14,965–14,991, doi:10.1029/1999JB900060.

Outerbridge, K. C., T. H. Dixon, S. Y. Schwartz, J. I. Walter, M. Protti, V. González, J. Biggs, M. Thorwart, and W. Rabbel (2010), A tremor and slip event on the Cocos-Caribbean subduction zone as measured by a global positioning system (GPS) and seismic network on the Nicoya Peninsula, Costa Rica, *J. Geophys. Res.*, *115*, B10408, doi:10.1029/2009JB006845.

Patino, L. C., M. J. Carr, and M. D. Feigenson (2000), Local and regional variations in Central American arc lavas controlled by variations in subducted sediment input, *Contrib. Mineral. Petrol.*, *138*(3), 265–283, doi:10.1007/s004100050562.

Payero, J. S., V. Kostoglodov, N. Shapiro, T. Mikumo, A. Iglesias, X. Perez-Campos, and R. W. Clayton (2008), Nonvolcanic tremor observed in the Mexican subduction zone, *Geophys. Res. Lett.*, *35*, L07305, doi:10.1029/2007GL032877.

Peacock, S. M. (2009), Thermal and metamorphic environment of subduction zone episodic tremor and slip, *J. Geophys. Res.*, *114*, B00A07, doi:10.1029/2008JB005978.

Peng, Z., and J. Gomberg (2010), An integrated perspective of the continuum between earthquakes and slow-slip phenomena, *Nat. Geosci.*, *3*, 599–607, doi:10.1038/ngeo940.

Peterson, C. L., and D. H. Christensen (2009), Possible relationship between nonvolcanic tremor and the 1998–2001 slow slip event, south central Alaska, *J. Geophys. Res.*, *114*, B06302, doi:10.1029/2008JB006096.

Plafker, G. (1976), Tectonic aspects of the Guatemalan earthquake of 4 February 1976, *Science*, *193*, 1201–1208, doi:10.1126/science.193.4259.1201.

Protti, M., F. Güendel, and K. McNally (1994), The geometry of the Wadati-Benioff zone under southern Central America and its tectonic significance: Results from a high-resolution local seismographic network, *Phys. Earth Planet. Inter.*, *84*, 271–287, doi:10.1016/0031-9201(94)90046-9.

Protti, M., et al. (1995), The March 25, 1990(M_w = 7.0, M_L = 6.8), earthquake at the entrance of the Nicoya Gulf, Costa Rica: Its prior activity, foreshocks, aftershocks, and triggered seismicity, *J. Geophys. Res.*, *100*(B10), 20,345–20,358, doi:10.1029/94JB03099.

Protti, M., M. F. Güendel, and E. Malavassi (2001), *Evaluación del Potencial Sísmico de la Península de Nicoya*, 1st ed., 144 pp., Ed. Fund. Univ. Nac., Heredia, Costa Rica.

Protti, M., V. González, T. Kato, T. Iinuma, S. Miyazaki, K. Obana, Y. Kaneda, P. LaFemina, T. Dixon, and S. Y. Schwartz (2004), A creep event on the shallow interface of the Nicoya Peninsula, Costa Rica seismogenic zone, *Eos Trans. AGU*, *85*(47), Fall Meet. Suppl., Abstract S41D-07.

Ranero, C. R., and R. von Huene (2000), Subduction erosion along the Middle America convergent margin, *Nature*, *404*, 748–752, doi:10.1038/35008046.

Ranero, C. R., J. Phipps Morgan, K. McIntosh, and C. Reichert (2003), Bending-related faulting and mantle serpentinization at the Middle America trench, *Nature*, *425*, 367–373, doi:10.1038/nature01961.

Rogers, G., and H. Dragert (2003), Episodic tremor and slip on the Cascadia subduction zone: The chatter of silent slip, *Science*, *300*, 1942–1943, doi:10.1126/science.1084783.

Rosencrantz, E., and P. Mann (1991), SeaMARC II mapping of transform faults in the Cayman Trough, *Geology*, *19*, 690–693, doi:10.1130/0091-7613(1991)019<0690:SIMOTF>2.3.CO;2.

Satake, K. (1994), Mechanism of the 1992 Nicaragua tsunami earthquake, *Geophys. Res. Lett.*, *21*(23), 2519–2522, doi:10.1029/94GL02338.

Savage, J. (1983), A dislocation model of strain accumulation and release at a subduction zone, *J. Geophys. Res.*, *88*(B6), 4984–4996, doi:10.1029/JB088iB06p04984.

Schmalzle, G., T. Dixon, R. Malservisi, and R. Govers (2006), Strain accumulation across the Carrizo segment of the San Andreas Fault, California: Impact of laterally varying crustal properties, *J. Geophys. Res.*, *111*, B05403, doi:10.1029/2005JB003843.

Schwartz, S. Y., and H. R. DeShon (2007), Distinct updip limits to geodetic locking and microseismicity at the northern Costa Rica seismogenic zone: Evidence for two mechanical transitions, in *The Seismogenic Zone of Subduction Thrust Faults*, edited by T. H. Dixon and J. C. Moore, pp. 576–599, Columbia Univ. Press, New York.

Shelly, D. R., G. C. Beroza, S. Ide, and S. Nakamula (2006), Low-frequency earthquakes in Shikoku, Japan, and their relationship to episodic tremor and slip, *Nature*, *442*, 188–191, doi:10.1038/nature04931.

Shelly, D. R., G. C. Beroza, and S. Ide (2007), Non-volcanic tremor and low-frequency earthquake swarms, *Nature*, *446*, 305–307, doi:10.1038/nature05666.

Siebert, L., and T. Simkin (2002), *Volcanoes of the World: An Illustrated Catalog of Holocene Volcanoes and Their Eruptions*, *Global Volcanism Program Digital Inf. Ser.*, vol. GVP-3, Smithsonian Inst., Washington, D. C. [Available at http://www.volcano.si.edu/world/].

Spinelli, G. A., and D. M. Saffer (2004), Along-strike variations in underhrust sediment dewatering on the Nicoya margin, Costa Rica related to the updip limit of seismicity, *Geophys. Res. Lett.*, *31*, L04613, doi:10.1029/2003GL018863.

Thomas, A. M., A. V. Newman, A. Ghosh, and G. T. Farmer (2007), Statistical modeling of the Middle America subduction zone using interplate seismicity, paper presented at Seismological Society of America Spring Meeting, Waikoloa, Hawaii.

von Huene, R., C. R. Ranero, W. Weinrebe, and K. Hinz (2000), Quaternary convergent margin tectonics of Costa Rica, segmentation of the Cocos Plate, and Central American volcanism, *Tectonics*, *19*(2), 314–334, doi:10.1029/1999TC001143.

Walter, J. I., S. Y. Schwartz, J. M. Protti, and V. González (2011), Persistent tremor within the northern Costa Rica seismogenic zone, *Geophys. Res. Lett.*, *38*, L01307, doi:10.1029/2010GL045586.

Wech, A. G., and K. C. Creager (2007), Cascadia tremor polarization evidence for plate interface slip, *Geophys. Res. Lett.*, *34*, L22306, doi:10.1029/2007GL031167.

Wessel, P., and W. H. F. Smith (1991), Free software helps map and display data, *Eos Trans. AGU*, *72*, 441, doi:10.1029/90EO00319.

White, R. A., and D. H. Harlow (1993), Destructive upper-crustal earthquakes of Central America since 1900, *Bull. Seismol. Soc. Am.*, *83*(4), 1115–1142.

Zumberge, J., M. Heflin, D. Jefferson, M. Watkins, and F. Webb (1997), Precise point positioning for the efficient and robust analysis of GPS data from large networks, *J. Geophys. Res.*, *102*(B3), 5005–5017, doi:10.1029/96JB03860.